# 15
# Imaging of Malignant Skeletal Tumors

**Jay Pahade, MD, Aarti Sekhar, MD, and Sanjay K. Shetty, MD**

## 1 Introduction

Malignant tumors of the skeleton represent a diverse group of primary and secondary neoplasms, each with unique imaging and clinical features. The radiologist encountering a lesion of the skeleton must apply a methodical approach to the analysis of imaging features to distinguish benign from malignant entities. This methodical approach can provide invaluable insight into the nature of the lesion, and will ultimately guide the final diagnosis; indeed, concordance between the imaging appearance and a preliminary histologic diagnosis is absolutely necessary to ensure that each lesion is appropriately diagnosed and managed. For the clinician, there is an ever-expanding array of potential imaging modalities that can characterize a lesion and evaluate its extent. Imaging will guide treatment, monitor response to therapy and facilitate discussions of prognosis.

The purpose of this chapter is to familiarize the practicing clinician and radiologist with the most common malignant lesions of the skeleton. The chapter describes the major primary lesions of bone (osteosarcoma, chondrosarcoma, myeloma, Ewing's Sarcoma and primary lymphoma of bone), as well as metastasis. Our goal is to familiarize the reader with the key imaging characteristics of each lesion, as well as the clinical features that may guide the differential diagnosis. The discussion incorporates all imaging modalities, including radiographs, magnetic resonance imaging (MRI), computed tomography (CT), positron emission tomography (PET) and bone scintigraphy, with a particular focus on the appropriate use of each modality in the diagnosis and staging of a newly detected lesion. Recent evidence, particularly focused on the newer modalities (MRI and PET), is presented to provide an evidence-based foundation for the imaging work-up.

Department of Radiology, Musculoskeletal Section, Beth Israel Deaconess Medical Center, Harvard Medical School, 330 Brookline Avenue, E/CC-4, Boston, MA 02215, 617-667-1658, Fax 617-667-8212

Direct correspondence to: SK Shetty, sshetty@bidmc.harvard.edu

M.A. Blake and M.K. Kalra (eds.), *Imaging in Oncology.*

## 2 General Approach: Radiographs

Radiographs are commonly the first imaging modality on which a skeletal lesion is detected and characterized. Despite the development of new imaging modalities, radiographs play a central role in the characterization of skeletal lesions. The majority of incidentally detected findings represent benign lesions, and it is the role of the radiologist to correctly differentiate these benign lesions to prevent the additional cost and morbidity associated with additional evaluation.

When evaluating a lesion several key features should be assessed to guide the differential diagnosis. The revised Lodwick classification system is a simple methodology for evaluating the margin and growth pattern of a bone lesion that provides insight into tumor growth rate and host response. This classification system divides lesions into geographic with sclerotic margins (grade IA), geographic with nonsclerotic margins, at most partial cortical destruction, and/or greater than 1 cm of cortical expansion (grade IB), geographic with full cortical penetration and at most 1 cm of a moth-eaten margin (grade IC), mixed geographic and moth-eaten (grade II), and permeative or moth-eaten (grade III). Key to this classification system is evaluation of the margin: a geographic lesion is one in which a pencil could easily be used to trace the margin. In contrast, a moth-eaten lesion will have irregular margins, often with numerous areas of lucency ("holes"), and a permeative lesion is extremely subtle and ill-defined. This grading system is important because of its predictive value; the rate of malignancy as defined in previous studies is: grade IA (6 percent), grade IB (48 percent), grade IC (36 percent), grade II (97 percent), and grade III (100 percent) [1, 2]. Lesions with a more aggressive appearance in this system should be considered malignant until proven otherwise, although it is important to keep in mind that benign entities (including infection and Langerhans Cell Histiocytosis) can have an aggressive appearance based on imaging alone.

Other characteristics can also help narrow the differential diagnosis. Location can be described in several ways: the affected bone (axial or appendicular skeleton, long or flat bone), location along the length of the bone (epiphyseal, metaphyseal or diaphyseal) and location within the bone (central, eccentric, cortical or juxtacortical). Internal matrix is either absent (no internal matrix), osseous (dense mineralization or cloud-like), chondroid (rings-and-arcs, popcorn) or fibrous (ground glass). Associated findings include the presence or absence of cortical destruction and endosteal scalloping, periosteal reaction and a contiguous soft tissue mass.

In discussing each of the major categories of malignant skeletal tumors, these imaging features will be referenced to help develop a framework for approaching these lesions from an imaging and clinical perspective.

# 3 Osteosarcoma

## *3.1 Introduction*

Osteosarcoma is the second most common primary bone tumor after multiple myeloma, accounting for 15 percent of all primary bone tumors. It is the most common bone tumor of young adults, coinciding with a period of increased bone development. While the etiology of osteosarcoma is unknown, the increased risk seen in patients with hereditary retinoblastoma and Li-Fraumeni syndrome suggests important pathogenetic roles of the tumor suppressor genes p53 and RB [3]. There is a predilection for males (gender distribution is 2:1) and the clinical presentation is usually nonspecific, with symptoms such as pain and swelling.

Histologically, osteosarcoma is an aggressive osteoid-producing lesion in the metaphyses of fast-growing long bones. The most common locations are the distal femur, proximal tibia, and proximal humerus. Even if elements such as fibrous or cartilage matrix dominate the tumor tissue, any production of an osteoid matrix confers the diagnosis of osteosarcoma. Pathologic fractures are seen in 15 to 20 percent of lesions, and approximately 20 to 25 percent of patients have metastases at the time of presentation [4]. The vast majority of these metastases are found in the lungs (90 percent) or bones [3]. Radiographic appearance is usually suggestive of the diagnosis of osteosarcoma. Key imaging findings include the presence of osteoid matrix and an overall aggressive imaging appearance, including aggressive periosteal reaction. CT and MRI can add critical information for staging and preoperative planning [4].

Numerous subtypes of osteosarcoma have been identified and characterized (see Table 15.1). This section focuses on the main subtypes of osteosarcoma, including intramedullary, surface and secondary osteosarcomas. Distinguishing between these subtypes requires characterizing the lesion in terms of patient demographics, location, and distinct imaging features. From the perspective of the imager, the correct identification of a particular subtype is particularly important when the distinction has therapeutic or prognostic impact.

## *3.2 Conventional or High Grade Osteosarcoma*

Conventional osteosarcoma, the most common subtype, is a large aggressive lesion affecting the metaphysis of long bones, particularly around the knee (Figs. 15.1, 15.2**).** The femur is most commonly involved (40 percent to 45 percent), followed by the tibia (16 percent to 20 percent) and the humerus (10 percent to 15 percent). The lesion usually starts in the metaphysis (90 percent to 95 percent), but often extends into the epiphysis, particularly when the physes are open. There is a slight male predilection, with a gender ratio of 1.5-2 to 1 [4].

**Table 15.1** Types of Osteosarcoma

| | |
|---|---|
| *I. Intramedullary (arise in medullary canal and occupy entire width of bone, usually higher grade)* | |
| High grade or conventional | 75% |
| Telangiectatic | 5-11% |
| Low grade | 5% |
| Small cell | 1-4% |
| Osteosarcomatosis or multifocal | 3-4% |
| Gnathic | 6-9% |
| *II. Surface or Juxtacortical (4-10% of all osteosarcomas, usually lower grade, arise in 3rd and 4th decade)* | |
| Intracortical | Rare |
| Parosteal | 5% (65% of surface osteosarcoma) |
| Periosteal | (25% of surface osteosarcoma) |
| High-grade | (10% of surface osteosarcoma) |
| *III. Secondary (5-7% of all osteosarcomas)* | |
| Paget | (67-90% of secondary osteosarcoma) |
| Post-radiation | (6-22% of secondary osteosarcoma) |
| Chronic infection, osteonecrosis, fibrous dysplasia | |
| *IV. Extraskeletal (4% of all osteosarcomas)* | |

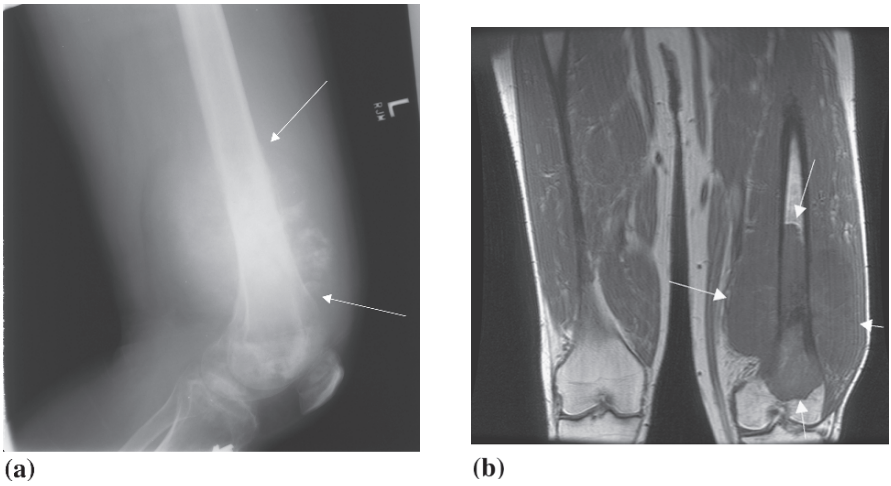

**(a)** **(b)**

**Fig. 15.1** Chondroblastic osteosarcoma in a 29-year-old male who presented with three months of persistent pain after trauma. (**a**) Lateral radiograph of the distal femur reveals a large, partially ossified lesion of the distal femur (arrows) with associated aggressive periosteal reaction. (**b**) Coronal T1-weighted and (**c**) sagittal T2-weighted MR images show a T1 isointense and T2 hyperintense mass of the distal femoral diaphysis and metaphysis with extraosseous extension (arrows). Note that the MRI clearly shows the extent of marrow involvement and clearly delineates associated soft tissue structures. (**d**) Frontal planar bone scintigraphy shows increased uptake in the distal femur, corresponding to the distal femoral mass (large arrow) and irregular uptake along the length of the tibia (small arrow) that reflects recent trauma. (**e**) Follow-up lateral radiograph after two cycles of neoadjuvent chemotherapy (methotrexate, Adriamycin, and cisplatin) demonstrates dense ossification of the mass. Images courtesy of Dr. Mary G. Hochman

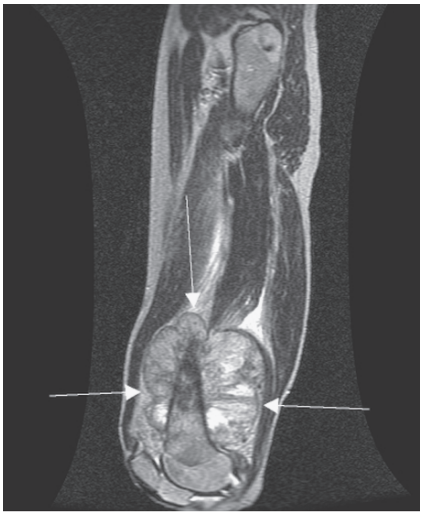

(c)

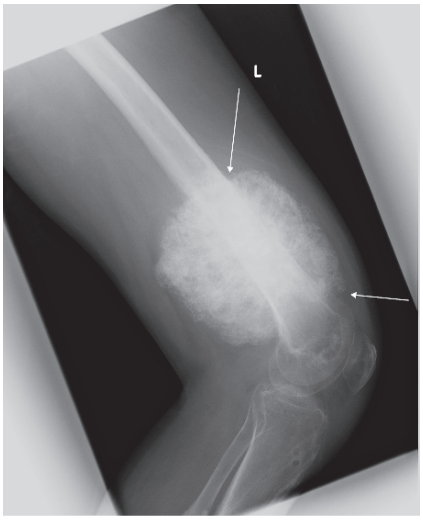


(e)

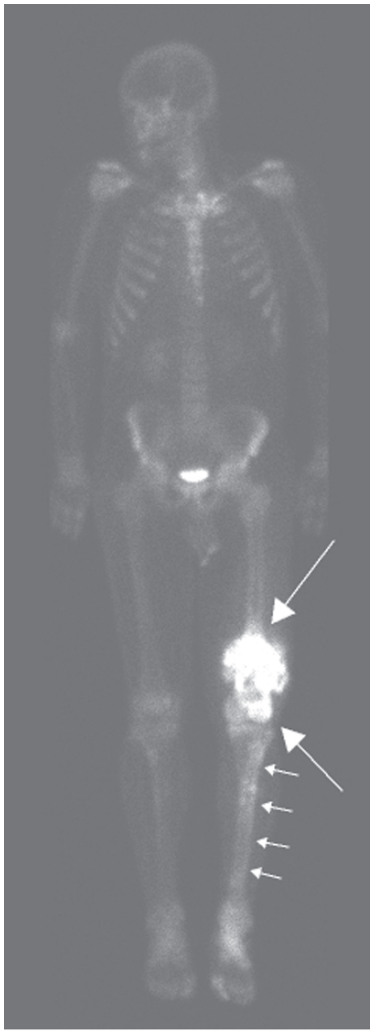

(d)

**Fig. 15.1** (continued)

Pathologically, osteosarcomas are usually large tumors (5 to 10 cm) with frequent soft tissue extension. They are comprised of mesenchymal cells that produce an osteoid matrix. Three histologic patterns are described depending on the predominant cell type: osteoblastic (50 percent to 80 percent), fibroblastic/fibrohistocytic (7 percent to 25 percent), and chondroblastic (5 percent to 25 percent). Osteosarcoma can also be graded from I to IV, depending on the degree of anaplasia and mitotic rate. Conventional osteosarcoma often achieves a grade of III to IV.

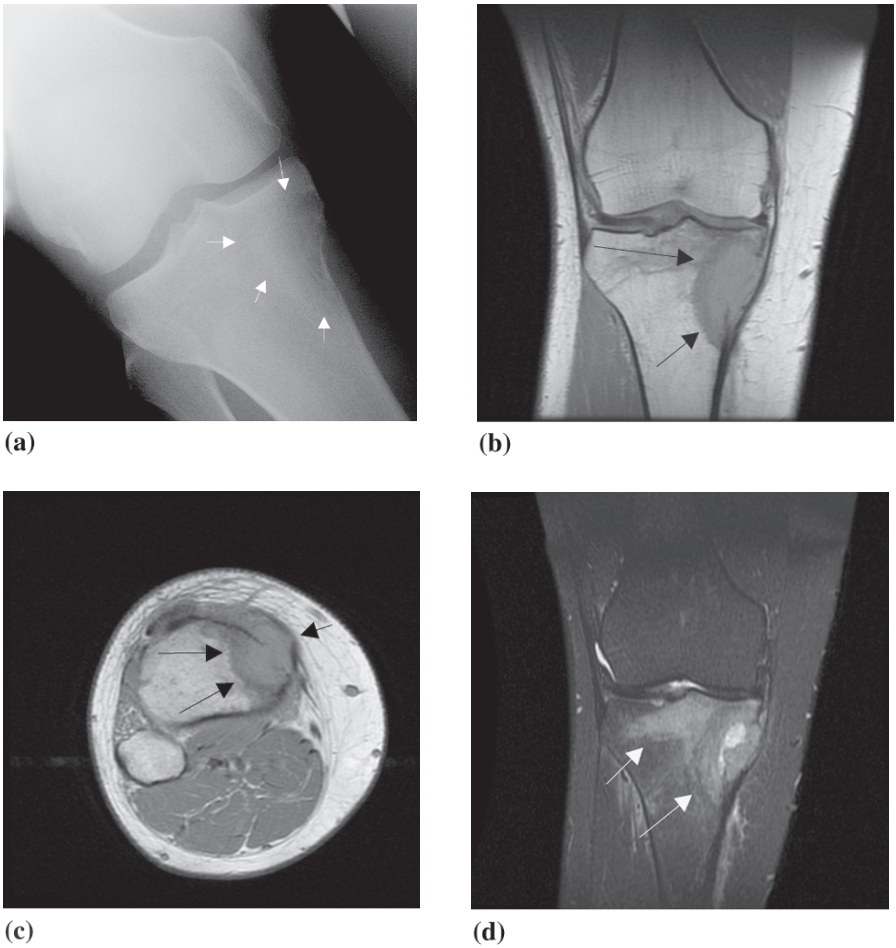


**Fig. 15.2** High-grade conventional osteosarcoma in a 21-year-old male presenting with knee pain. (**a**) Frontal radiograph of the right knee demonstrates an ill-defined lucent lesion of the proximal tibial epiphysis / metaphysis (white arrows) with medial cortical destruction. (**b**) Coronal and (**c**) axial proton density weighted and (**d**) coronal STIR MR images of the proximal tibia better show the extent of marrow involvement and the extraosseous extension through a violated cortex (arrows). Images courtesy of Dr. Mary G. Hochman

Radiographic characteristics include a mixed lytic-sclerotic pattern with a variable amount of fluffy, cloud-like opacities within the lesion representing osteoid matrix. Cortical breakthrough without expansion of the bone and an aggressive periosteal reaction with a laminated, hair-on-end or sunburst appearance are common. Soft tissue masses are seen in 80 to 90 percent of lesions [4, 5]. Poor prognostic factors include tumor size > 10 cm, advanced stage at presentation, and pathologic fracture [4].

CT imaging is useful in defining the extent of tumor, evaluating anatomically complex areas (pelvis, mandible, maxilla), and characterizing small lesions that measure < 5 cm. Additionally, CT offers superior detection of subtle areas of mineralized matrix in mostly lytic lesions. On CT imaging, the tumor will be primarily low attenuation or soft tissue density, with areas of higher attenuation osteoid production. When there is extensive edema or necrosis, CT scanning may be superior to MRI for determining soft tissue involvement.

Osteosarcoma shows marked uptake of radiotracer on bone scintigraphy; however, the pattern of uptake is nonspecific. The main role for scintigraphy is in evaluating for distant metastases, both osseous and extraosseous, including ossified pulmonary metastases.

MRI is important for preoperative evaluation and staging, particularly for assessing the extent of marrow, soft tissue, epiphyseal, neurovascular and joint involvement [4, 5] (Fig. 15.3). It also allows better identification of viable tumors to improve biopsy accuracy. A tumor is seen as low to intermediate signal intensity on T1-weighted images and high signal intensity on STIR or T2-weighted images. Areas of low signal intensity on T1 and T2 images represent mineralized matrix, and areas of high signal intensity on both T1- and T2-weighted images can represent hemorrhage. Necrosis can be seen as low signal intensity on T1 and high signal intensity on T2. MRI should be performed before neoadjuvant chemotherapy, since edema can be misinterpreted as tumor, particularly on STIR images. MRI can also readily identify skip lesions, which are rare (occurring in < 5 percent of conventional osteosarcomas), but are important to identify because they necessitate a more extensive resection and are associated with an extremely poor prognosis [6].

There is currently insufficient data regarding the use of PET/CT in the evaluation and follow-up of osteosarcoma. However, preliminary work has been promising, suggesting that FDG-PET may be useful for the characterization of biologic features of osteosarcoma that relate to tumor grading and treatment follow-up [7].

Treatment of high-grade intramedullary osteosarcoma includes neoadjuvant chemotherapy followed by limb-salvage procedures and postoperative multi-drug chemotherapy, leading to a five-year survival rate of 60 percent to 80 percent.

## *3.3 Telangiectatic Osteosarcoma*

Telangiectatic osteosarcoma is an uncommon variant, comprising 5 to 11 percent of osteosarcomas. It is characterized by cystic cavities with cavernous vessels and blood-filled spaces. Osteoid matrix can sometimes be seen in the periphery of the lesion or in the septations of these cavities.

Like high-grade intramedullary osteosarcoma, the telangiectatic variant most commonly affects the metaphyseal regions of the long bones around the knee (48 percent in the distal femur and 14 percent in the proximal tibia), with the proximal humerus also being common (16 percent) [8]. The classic radiographic appearance is a large lytic and expansile lesion (mean lesion size is 6.8 × 11.2 cm) that is occasionally

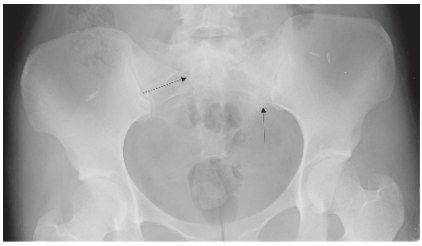

(a)

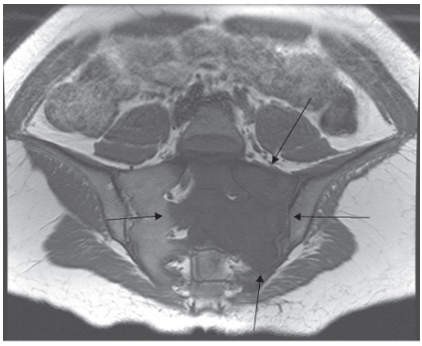

(c)

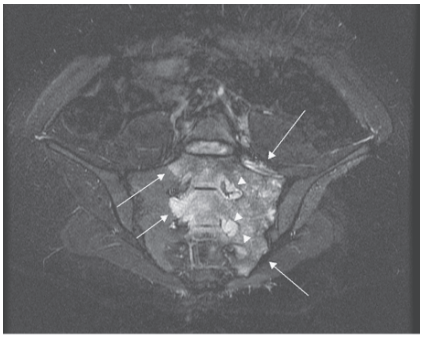

(d)

(b)

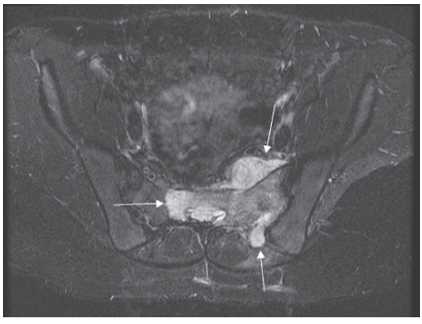

(e)

markedly aneurysmal and can mimic an aneurysmal bone cyst. Multiple small fluid/fluid levels, best seen on MRI, are a characteristic finding of telangiectatic osteosarcomas that also mimic aneurysmal bone cysts. The key distinguishing feature is that the telangiectatic osteosarcoma will have a rim of viable tumor cells along the periphery of its cystic spaces, seen best on contrast-enhanced CT and MRI as thick nodular peripheral enhancement [9].

Aggressive features such as cortical destruction (in a geographic pattern), periosteal reaction, wide zone of transition, and pathologic fracture are common [4, 9]. Contrast-enhanced CT shows a marrow-replacing lesion with heterogeneous attenuation. MRI shows very heterogenous signal intensity that is intermediate to high signal intensity on T1-weighted images, and high on T2-weighted images, with evidence of hemorrhage on all MRI pulse sequences. Both CT and MRI contrast-enhanced imaging show thick peripheral and septal enhancement, corresponding to areas of sarcomatous tissue and osteoid matrix (the latter of which is optimally seen on CT). Biopsy should be directed towards these peripheral nodules. Soft tissue masses are also frequently seen on CT and MRI.

Bone scintigraphy shows marked radionuclide uptake with central photopenia (termed the "donut pattern"), corresponding to a hemorrhagic center. Angiography, which is not routinely performed, can show a hypervascular peripheral stain with or without early venous drainage [9].

Telangiectatic osteosarcoma previously had a dismal prognosis, until the advent of chemotherapy. Now, prognosis is comparable to conventional osteosarcoma [10]. With chemotherapy and wide surgical resection, the five-year survival rate is 68 percent [4].

## *3.4 Low Grade Osteosarcoma*

Low-grade osteosarcoma comprises 5 percent of intramedullary osteosarcomas and affects patients most commonly in the third decade of life. Distribution is most commonly in the metaphyseal region around the knee. Pathologically and radiographically, low-grade osteosarcoma simulates a benign process, including NOF, fibrous dysplasia, and chondromyxoid fibroma. The lesion can show well-defined sclerotic margins, with only subtle evidence of a more aggressive process, such as

**Fig. 15.3** Sacral chondroblastic osteosarcoma in a 25-year-old who presented with left leg numbness. (**a**) AP radiograph of the pelvis demonstrates a very subtle ill-defined sclerosis involving the left sacrum (arrows). (**b**) Technicium-99 m bone scintigraphy demonstrates a focus of intense tracer uptake within the left sacrum, without distant osseous metastases. (**c**) Coronal T1, (**d**) coronal STIR, and (**e**) axial STIR MR images shows a large infiltrative mass that is T2 hyperintense and T1 isointense to muscle involving the left side of the sacrum at the S1 and S2 levels. The mass extends across midline, into the ventral soft tissues, and into the S1, S2, and S3 neural foramina (arrowheads)

small areas of cortical destruction and an associated soft tissue mass. This variant has locally aggressive behavior and will often recur unless a wide excision is performed. With complete resection, prognosis is excellent.

## 3.5 Small Cell Osteosarcoma

Small cell osteosarcoma, which accounts for 1 percent to 4 percent of osteosarcomas, is composed of small round blue cells. Histologically, these tumors are similar to Ewing's sarcoma except that small cell osteosarcoma produces an osteoid matrix and lacks the cellular uniformity seen in Ewing's. However, some investigators consider this tumor a Ewing's variant, especially those tumors with positive CD99 membrane staining and chromosome 11-22 translocation, which are classic findings for Ewing's sarcoma [10].

Again, the metaphysis of the distal femur is the most common location, followed by the proximal humerus and the pelvis. Imaging findings are nonspecific for small cell osteosarcoma (usually diagnosed by biopsy), but findings are similar to conventional osteosarcoma and suggest a highly aggressive lesion. These lesions can be permeative, lytic, and have aggressive features such as cortical breakthrough, aggressive periosteal reaction and soft tissue extension, the latter of which is best seen on cross-sectional imaging. Intramedullary sclerosis is also common. Prognosis is extremely poor [4, 11].

## 3.6 Gnathic Osteosarcoma

Gnathic osteosarcoma is an osteoid-producing tumor of the mandible and maxilla that is predominantly chondroblastic and affects a slightly older population (average age 34 to 36 years). These tumors are difficult to image and treat, due to the complex anatomic location. CT is often needed to detect the osteoid matrix. Opacification of the maxillary sinus is commonly seen in maxillary lesions. Treatment consists of surgical resection, radiation, and chemotherapy. Local recurrence is common, and the tumor carries a five-year survival rate of only 40 percent.

## 3.7 Intracortical Osteosarcoma

Intracortical osteosarcoma, first described by Jaffe in 1960, is the rarest subtype of osteosarcoma, with only a handful of cases reported in the literature [12]. The lesion is typically a cortically based lytic lesion that is $< 4$ cm in diameter and has a rim of perilesional sclerosis. The femur and tibia are, again, the most common location [12].

## 3.8 Parosteal Osteosarcoma

Parosteal osteosarcoma, the most frequent type of surface lesion (comprising 65 percent of surface osteosarcomas) originates from the outer layer of the periosteum. Patients are usually in the third to fourth decade of life and present with a palpable mass in their distal posterior thigh. The lesion is typically a large lobulated cauliflower-like juxtacortical mass arising from the metaphyseal region of long bones. A histologically low-grade tumor with possible high-grade regions within it, parosteal osteosarcoma occasionally demonstrates "back-growth" invasion into the medullary canal.

Radiographically, parosteal osteosarcoma presents as a large centrally dense lesion, attached to the underlying bone by a stalk in earlier stages and with a broader base later in the progression of the disease. The classic location is the posterior distal femur (50 percent to 65 percent of cases). Cortical thickening without an aggressive periosteal reaction is common. Because of its appearance as an ossified mass outside of the bone, parosteal osteosarcoma must be differentiated from myositis ossificans, a lesion that is denser peripherally and not attached to the cortex. Additionally, a cartilage cap is seen in 25 percent to 30 percent of lesions, which may lead to mis-diagnosis as osteochondroma [10].

CT can be useful in demonstrating a radiolucent zone of periosteum and fibrous tissue that becomes trapped between the encircling tumor and cortex. MRI can define the extent of tumor extension to ensure complete surgical resection. Parosteal osteosarcoma has an excellent prognosis and is usually treated with local resection [4, 10]. There is a rare dedifferentiated variant, with a much poorer prognosis.

## 3.9 Periosteal Osteosarcoma

Periosteal osteosarcoma is a rarer surface lesion arising from the deep layer of periosteum of the femur, tibia, or humerus. Radiographically, these lesions present as a diaphyseal lesion with a thickened, scalloped cortex (without intramedullary invasion), involving over 50 percent of the osseous circumference and displaying a perpendicular periosteal reaction. This periosteal reaction can be seen as rays of low signal intensity on all MRI sequences. These lesions are considered intermediate grade with a fair prognosis. Treatment usually involves wide surgical resection.

## 3.10 High-grade Surface Osteosarcoma

High-grade surface osteosarcoma are rare tumors that are histologically identical to high-grade intramedullary osteosarcoma and radiographically similar to periosteal osteosarcoma. Often the entire circumference of the bone is involved. There is controversy over whether these lesions can invade the medullary canal

[4, 10]. Aggressive (hair-on-end) periosteal reaction has also been observed. The diaphysis of the femur, humerus, or fibula is involved. Prognosis and treatment are similar to conventional intramedullary osteosarcoma.

## *3.11 Multifocal Osteosarcoma*

Multifocal osteosarcoma is a rare subtype which affects children in the first decade of life and is rapidly fatal. This entity is thought to be a metastatic process involving a dominant lesion with aggressive features, and multiple secondary foci that are smaller and more benign-appearing (sclerotic with well-defined margins). Pulmonary metastases are often seen with this subtype.

## *3.12 Secondary Osteosarcoma*

Osteosarcoma can also result from malignant transformation of a benign process and is seen most frequently in the setting of Paget's disease (67 percent to 90 percent) (Fig. 15.4) and previous radiation (6 percent to 22 percent) of greater than 1,000 cGy [4]. Other entities that have been reported to uncommonly predispose to osteosarcomatous degeneration include fibrous dysplasia and multiple chondromas.

Patients with Paget's disease tend to be older (typical age range: 55 to 80 years) and malignant transformation to osteosarcoma is suggested by new and progressive bone pain. There is large variation in the frequency of malignant transformation, depending on the extent of disease: patients with limited disease have only a 0.2 percent frequency of transformation, while the figure can be as high as 7.5 percent in those with extensive skeletal disease. Radiographically, aggressive bony destruction can be seen in the setting of the bony sclerosis and expansion that is characteristic of Paget's disease. The most common sites of disease include the femur, pelvis, humerus, and craniofacial bones. Soft tissue masses are common. These lesions are high-grade and aggressive, with an extremely poor prognosis and five- to ten-year survival rate of less than 5 percent. The dismal prognosis is also a reflection of the poor health of the older population affected by the tumor, surgically inaccessible tumor sites and increased vascularity of the bone, which predisposes to hematologic metastases, particularly to the lungs [4, 13].

## *3.13 Osteosarcoma: Staging*

Prognosis for osteosarcoma is determined by histologic grade and the site of the lesion. The presence of metastases confers a much poorer prognosis, and may require more intensive chemotherapy regimens that have their own risk, including

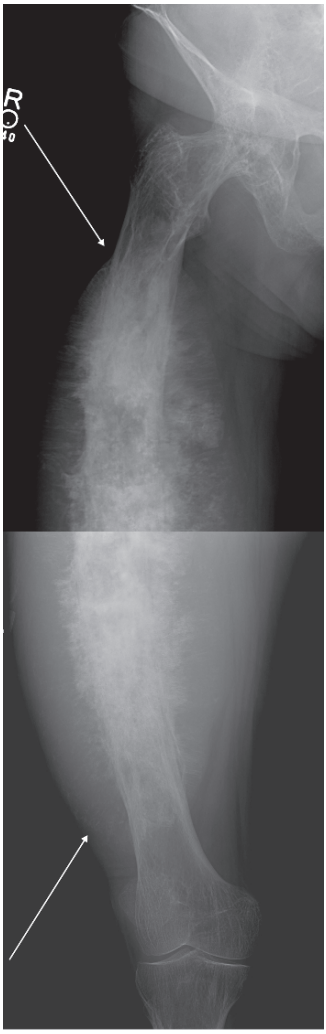

(a)

(b)

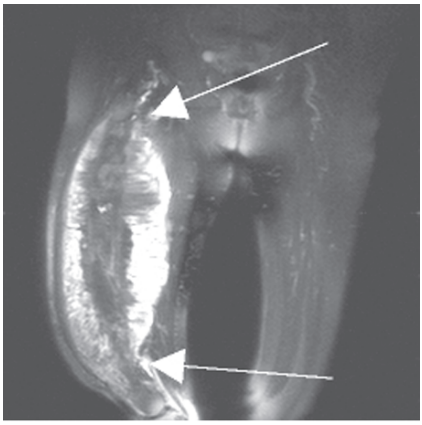

(c)

**Fig. 15.4** Secondary osteosarcoma in a 63-year-old female, occurring in the setting of Paget's disease. (**a**) Composite frontal radiographs of the right femur demonstrate underlying Paget's disease with cortical thickening and trabecular coarsening involving the proximal femur. A large secondary osteosarcoma is seen within the diaphysis, with "hair-on-end" periosteal reaction and an extensive ossified soft tissue component. (**b**) Coronal HASTE (T2) and (**c**) coronal HASTE (T2) with fat saturation reveal an expansile mass arising from the diaphysis of the right femur, extending from the lesser trochanter to the distal metaphysis. Extensive abnormal periosteal reaction and internal osseous matrix (low signal) are seen. The muscle groups of the thigh are displaced peripherally in all directions

high-dose alkylating agents which can increase risk for leukemia [3]. However, in general, neoadjuvant chemotherapy has dramatically improved survival rates for osteosarcoma, thus increasing the demands for imaging to provide detailed information on tumor staging and grading. Currently, staging for osteosarcoma includes conventional radiography of the lesion and biopsy for definitive diagnosis; MRI of the tumor and surrounding bone to assess the extent of disease and evaluate for skip lesions; high-resolution CT (HRCT) of the chest to evaluate for pulmonary metastases; and bone scintigraphy to evaluate for distant bone metastases [7, 14]. There is currently insufficient data on the role of PET/CT in staging of osteosarcoma [7].

Treatment involves neoadjuvant chemotherapy followed by wide local excision with limb-salvage procedures and postoperative chemotherapy, leading to a cure rate ranging from 58 percent to 76 percent [4]. Complete resection with negative margins at the initial surgery is crucial, as positive margins correlate with an increased likelihood of local recurrence, and a subsequently poor prognosis (five-year survival rate of 19.2 percent) [15].

Chemotherapy has become increasingly important in curbing hematologic spread and preventing lung metastases. In addition, response to chemotherapy is one of the most important prognostic factors: greater than 90 percent necrosis after chemotherapy is associated with a significantly higher survival rate. Radiation therapy should be used conservatively in the young population affected by osteosarcoma as these tumors are relatively insensitive to radiation, and there is an increased risk of secondary osteosarcoma and radiation-induced soft tissue sarcomas [3].

## *3.14 Osteosarcoma: Follow-up*

Patients should be followed closely for local and systemic recurrence. Local recurrence confers a much poorer prognosis. For pulmonary metastases that are detected early, surgical removal of these lesions can confer a 20 percent to 50 percent chance of cure [7]. There is no established follow-up regimen. Some authors advocate plain radiographs of the affected extremity and HRCT of the chest every three to six months for the first two years following surgery, every six months for the second through fifth year, and then annual surveillance exams. Annual bone scintigraphy is recommended for the first two years [16]. Others advise follow-up with bone scintigraphy alone, since osteosarcomas usually incorporate bisphosphonates, and HRCT of the chest at six-month intervals [7]. Prostheses should also be evaluated for loosening, infection, and mechanical failure.

In evaluating for local response to chemotherapy and local recurrence, modalities that evaluate morphologic changes (such as radiographs and CT) have been shown to be of limited value. Thallium-201 scintigraphy, which reflects tumor metabolic activity, has proven itself to be a powerful tool in monitoring tumor response to induction chemotherapy and for detecting local recurrence [17, 18]. MRI is also useful in evaluating treatment response due to its superior soft tissue

contrast and the sensitivity for detection of enhancement following gadolinium administration, which may help distinguish viable from necrotic tumor. There is also considerable interest in the role of functional imaging, such as PET/CT, for following response to therapy. PET/CT may help target biopsy in large heterogeneous tumors by delineating highly metabolically active areas [7]. Bredella, et al. showed PET/CT to be helpful in distinguishing viable tumors from post-therapeutic changes when MRI was equivocal [19]. However, there is conflicting evidence from several small studies regarding correlation between SUV measurements and histologic response after chemotherapy [7, 20]. One major pitfall of PET is poor sensitivity for detection of pulmonary metastases, particularly those that are less than 9 mm, the detection of which can significantly improve survival. Larger prospective trials are needed to define the role of PET/CT in the management of osteosarcoma.

### *3.15 Osteosarcoma: Summary*

Osteosarcoma is the most common primary bone tumor of young adults and is defined as any primary bone tumor with production of an osteoid matrix. It commonly occurs in the bones surrounding the knee joint and in the proximal humerus. A variety of subtypes have been described, each with characteristic radiologic features and widely varying prognoses. The most common subtype, conventional or intramedullary osteosarcoma, is a high-grade tumor characterized by cortical destruction, strong periosteal reaction, and associated soft tissue mass.

Diagnostic work-up of osteosarcoma includes tumor characterization by radiographs and MRI, image-guided biopsy, evaluation of pulmonary metastases with HRCT of the chest, and bone scintigraphy to evaluate for bony metastases. Treatment involves neoadjuvant chemotherapy followed by wide local excision with limb-salvage therapies and postoperative chemotherapy. Chemotherapy has considerably improved survival rates in osteosarcoma over the past decade. Follow-up evaluation, including imaging of the affected area and HRCT of the chest, is crucial for early detection of local recurrence and metastasis. PET/CT remains an unproven but promising tool in assessing post-therapy response and residual disease.

## 4 Chondrosarcoma

### *4.1 Introduction*

Chondrosarcoma is a malignant tumor of bone characterized by cells that produce a cartilaginous tumor matrix. It is generally classified as primary or secondary on the basis of whether the cells arise de novo (primary) or are superimposed on a

preexistent benign condition such as enchondroma or osteochondroma (secondary). Regional classification systems divide chondrosarcomas based on osseous location into central or peripheral. Central defines tumors that are intramedullary in origin, including those with peripheral extension. Peripheral tumors are further subdivided into those that are secondary, arising from a preexisting osteochondroma, and juxtacortical, which arise from the bone surface [21].

Chondrosarcoma is the third most common type of primary malignant bone tumor. It is estimated to represent 20 percent to 27 percent of all primary malignant bone neoplasms [21]. Syndromic associations with increased risk of chondrosarcoma include the enchondromatosis syndromes (Ollier disease and Maffucci syndrome) and Hereditary Multiple Exostoses (HME).

Primary chondrosarcoma is a broad term encompassing many pathologic subtypes with distinct clinical and radiological characteristics. We will discuss conventional intramedullary, clear cell, juxtacortical, myxoid, mesenchymal and dedifferentiated subtypes in this chapter. Radiographs or CT can often suggest the cartiligenous nature of these lesions, demonstrating a predominant chondroid matrix mineralization (termed "arcs-and-rings"). The key role of radiographic work-up is to characterize individual lesions (including assessment of benign and malignant features). The combined multimodality use of radiographs, bone scintigraphy, PET, CT, and MRI scanning can help with staging and guidance of surgical resection and overall treatment.

## *4.2 Conventional Intramedullary Chondrosarcoma*

Conventional intramedullary chondrosarcoma (central chondrosarcoma) is the most common type of primary chondrosarcoma [21]. Patients most frequently present in the fifth and sixth decades and there is a 1.5-2 fold male predilection. Insidious, progressive pain that is worse at night is often the chief complaint; patients complain of pain in at least 95 percent of cases at presentation (Figs. 15.5, 15.6). Palpable mass is sometimes present. Pathologic fractures may often be the initial findings, occurring in 3 to 17 percent of patients [21]. New onset pain should also suggest the possibility of malignant degeneration of benign lesions such as enchondromas and ostechondromas, although pain may also be caused by local impingement or pathologic fracture and does not in itself reflect malignancy. Malignant lesions can also be clinically silent and detected incidentally [22].

Skeletal location can help differentiate conventional intramedullary chondrosarcoma from other subtypes. The proximal aspect of long tubular bones are most commonly affected, particularly the femur (20 percent to 35 percent of cases), upper extremity (10 percent to 20 percent, usually proximal humerus), and tibia (5 percent). The axial skeletal is also frequency affected, with the pelvic bones accounting for approximately 25 percent of lesions and ribs accounting for 8 percent. Any bone can be affected by conventional chondrosarcoma, including the spine, sesamoids and short tubular bones of the hand and feet [21]. In the long

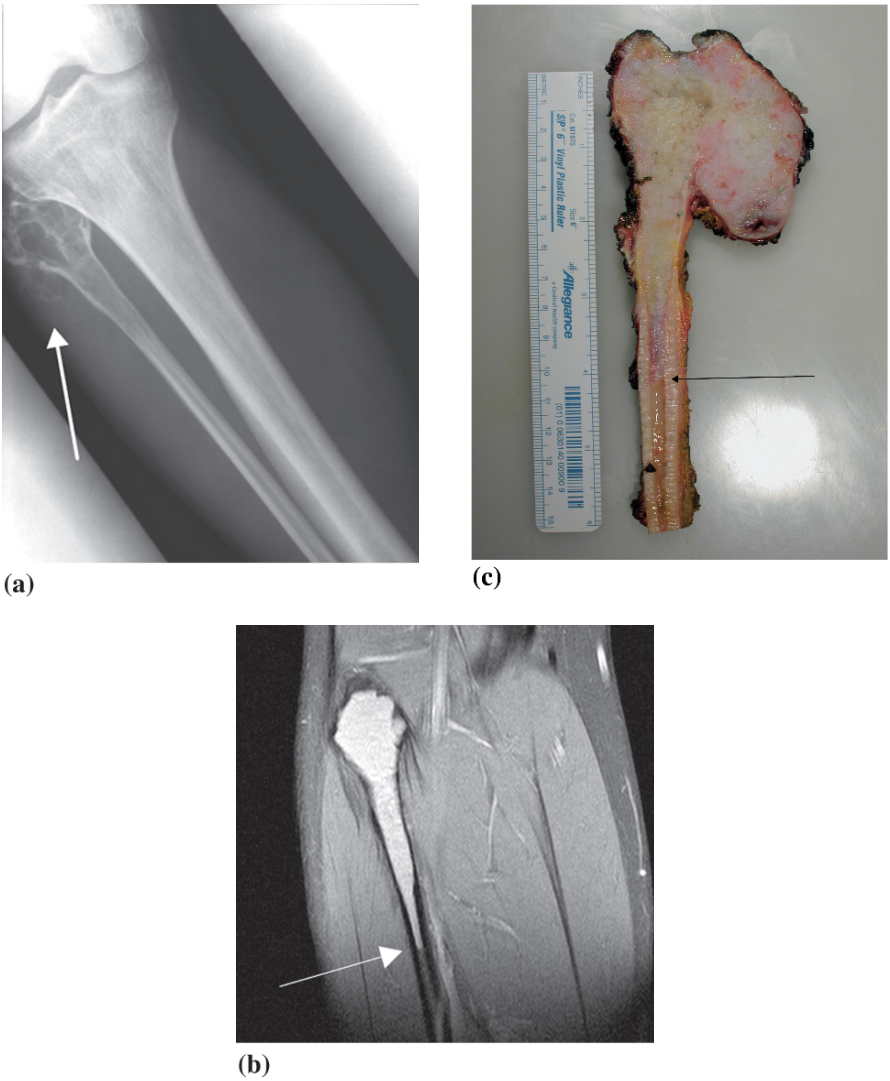


**Fig. 15.5** Low-grade conventional chondrosarcoma. (**a**) Radiograph displays mostly lytic lesion involving the proximal fibula. Note the focal cortical destruction, expansion of the proximal fibula, endosteal scalloping extending along the fibular shaft and the faint "arcs-and-rings" cartilaginous matrix (arrow) in the adjacent soft tissues reflecting the extraosseous extension of the mass. (**b**) Coronal STIR MRI image reveals the hyperintense cartilagenous internal structure and the extension of the mass along the fibular shaft. (**c**) Pathologic specimen shows the full mass, including the soft tissue component and the distal extension of the mass along the fibular shaft (arrow)

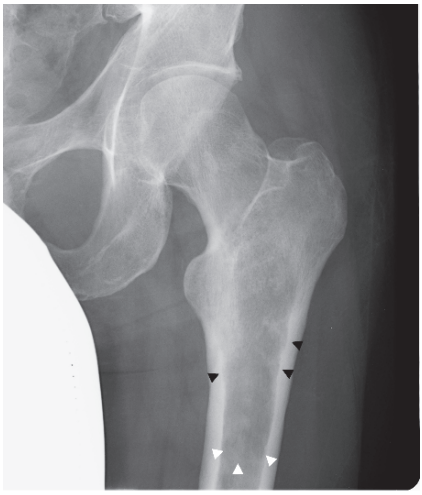

(a)

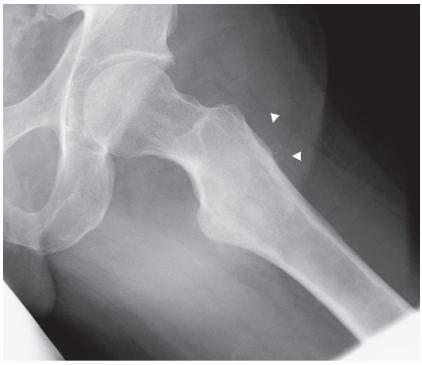

(b)

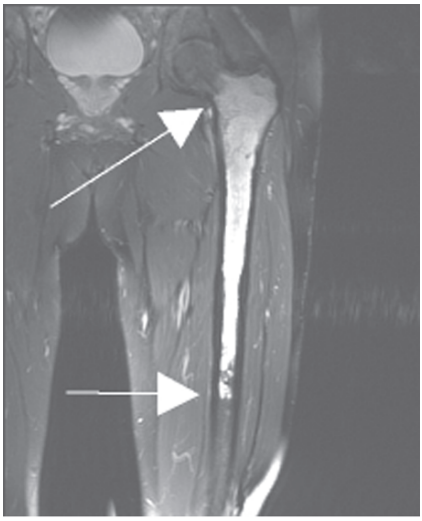

(c)

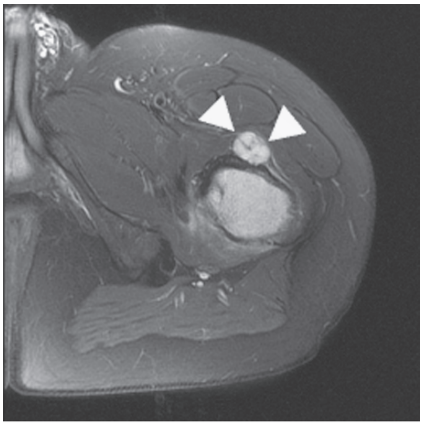

(d)

**Fig. 15.6** Intermediate grade chondrosarcoma in a 41-year-old male presenting with vague hip pain. (**a**) Frontal radiograph shows a subtle lucent lesion in the proximal femur with extension distally into the proximal diaphysis (white arrowheads) and endosteal scalloping (black arrowheads). (**b**) Frog-leg lateral radiograph reveals a focal area of cartilagenous matrix in the adjacent soft tissues, suggesting extraosseous extension. (**c**) Coronal and (**d**) axial STIR MR images show the full extent of involvement within the femoral shaft (arrows) and the nodules of extraosseous extension (arrowheads)

bones, the metaphysis and diaphysis are involved in 49 and 36 percent of cases, respectively. Only 16 percent of cases are centered in the epiphysis [23].

Chondrosarcomas typically display a mixed lytic and sclerotic pattern, with the sclerotic pattern representing chondroid matrix mineralization. "An arcs-and-rings" pattern of mineralization is the classic description, although on occasion this mineralization may coalesce into a denser pattern. The chondroid matrix pattern of calcification often allows confident diagnosis of a cartilaginous lesion. The lytic component of the lesion often suggests the grade of tumor, a characteristic which correlates well with outcome [24]. The initial histologic grading system was initially suggested by Evans and colleagues [25]. Grade I (low-grade) lesions possess a predominantly chondroid stroma with sparse myxoid areas and chondrocytes with small dense nuclei. Grade II have less chondroid matrix and are more cellular, frequently with myxoid stroma. Grade III (high-grade) lesions exhibit greater cellularity with little to no chondroid matrix and small intercellular myxoid material. High-grade lesions display less chondroid matrix calcification with the radiolucent component displaying a more aggressive pattern of geographic multilobulated bony lysis [21].

Low-grade chondrosarcoma continues to be the most difficult lesion to differentiate from benign cartilaginous lesions [22, 26] in terms of both imaging and histology. Even percutaneous biopsy is subject to sampling error that may fail to identify focal regions of sarcoma. In practice histologic analysis of the entire lesion (following resection) may be necessary to definitively characterize the lesion as benign or malignant. Investigators have attempted to establish imaging parameters to distinguish the two entities, employing a variety of modalities. Endosteal scalloping (erosion of the inner cortex) leading to cortical penetration and soft tissue extension are frequently associated with conventional chondrosarcomas. The depth of scalloping may serve as one of the best distinguishing features between a chondrosarcoma and benign enchondroma: endosteal scalloping involving greater then two-thirds of the normal thickness of cortex is strong evidence of chondrosarcoma as it was identified in 75 percent of cases of chondrosarcoma, versus 9 percent of enchondromas [23]. Another distinguishing feature is the longitudinal extent of endosteal scalloping: chondrosarcoma typically has scalloping involving the entire length of the lesion versus partial involvement in enchondroma [23]. Cortical destruction is an important characteristic: up to 88 percent of conventional chondrosarcomas display cortical destruction, compared to only 8 percent of enchondromas. Soft tissue involvement essentially rules out the diagnosis of enchondroma [23]. Recent work has also suggested that analysis of chromosomal abnormalities may be able to reliably diagnose grade I chondrosarcoma [27].

Traditional work-up for a conventional intramedullary chondrosarcoma usually involves multimodality imaging to better define the osseous and soft tissue characteristics. CT possesses an inherent benefit relative to radiographs when defining osseous involvement, matrix pattern, depth and extension of endosteal scalloping, and particularly in demonstrating cortical destruction. Contrast-enhanced scanning generally shows the lesion's peripheral rim and septal enhancement [21].

MRI provides the best assessment of marrow involvement. T1-weighted images display low to intermediate signal intensity in areas with marrow replacement relative to the high signal medullary fat. Focal areas of high T1 signal within the lesion, representing unaffected areas of marrow, is a more common feature of benign lesions, identified in 35 percent of conventional chondrosarcomas versus 65 percent of enchondromas [21]. Unmineralized portions of conventional chondrosarcomas display high signal intensity on T2-weighted images reflecting the high water content of hyaline cartilage. Matrix mineralization is better visualized via CT or radiographs and displays low signal on all MRI pulse sequences creating a heterogeneous pattern on T2-weighed sequences. Similar T2 patterns can also be identified in fibrous tissue with high collagen content or other types of generalized calcification [21]. MRI is superior to other modalities in its ability to identify soft tissue extension due to its superior soft tissue contrast. Approximately 76 percent of conventional chondrosarcomas display soft tissue extension, essentially excluding enchondroma [23]. Most agree that a larger soft tissue mass tends to be associated with a higher grade lesion. Often the soft tissue component displays similar imaging intrinsic characteristics as the intraosseous component. Peritumoral edema, identified on water sensitive MRI sequences, may also suggest the diagnosis of conventional chondrosarcoma versus enchondroma [28].

MRI enhancement patterns have been evaluated by several studies with mixed results. Nevertheless, enhancement patterns can suggest the diagnosis of chondrosarcoma versus an osteochondroma. Peripheral enhancement is typically seen in osteochondromas, though it can occasionally be seen in low-grade chondrosarcomas. High-grade chondrosarcomas, on the other hand, have a more diffuse enhancement pattern which can be homogeneous or heterogeneous [29]. Septal enhancement can be seen in both benign osteochondromas and low-grade chondrosarcoma [30, 31]. Subtraction MRI has revealed early and progressive enhancement in chondrosarcomas. When used in combination, these enhancement patterns may help differentiate malignant from benign lesions with increased certainty [31]. Enhancement patterns may also help pinpoint the most appropriate target for percutaneous biopsy.

Bone scintigraphy will typically display increased tracer uptake in chondrosarcoma. However, the findings are not specific for the diagnosis, and up to 21 percent of enchondromas also show increased uptake. A heterogeneous uptake pattern may help better distinguish the two entities; 63 percent of intramedullary chondrosarcoma display this pattern versus 30 percent of enchondromas [23].

The role of $^{18}$FDG-PET is still being evaluated in clinical practice; however preliminary results appear favorable in using PET – or combination PET/CT – in initial diagnosis, detection of metastasis, and follow-up evaluation in chondrosarcoma [22]. While literature focused solely on PET for conventional intramedullary chondrosarcoma is scarce, several reviews have included multiple subtypes of chondrosarcoma. PET cannot reliably differentiate benign enchondroma from Grade I chondrosarcoma on the basis of SUV (standard uptake values) alone. However, PET may have a role in the classification of lesions as high-grade Grade II to III chondrosarcomas, as SUV values are significantly higher than in benign

cartilaginous lesions. It has been suggested that a SUV value above 2.3 be the benchmark to characterize high-grade lesions, although there are case reports of benign lesions (such as giant cell tumors) displaying SUV values above 3. While some series have suggested that PET can reliably distinguish low-grade and high-grade chondrosarcoma [24], others have found overlap in maximal SUV values that preclude definitive separation of Grade I and Grade III tumors [32]. In one series, Grade I central medullary chondrosarcomas had a maximum SUV of 4.1 with a mean value of 2.8, which can overlap with higher grade lesions [32]. Tumor size did not reliably affect SUV values, as larger tumors do not necessarily have higher standardized uptake values than the smaller tumors [24, 32]. PET may play a more prominent role in detecting and evaluating metastases, as SUV values have been found to be extremely high [24]. The role of PET in predicting outcomes has also been investigated; pre-therapeutic tumor maximal SUV obtained by quantitative FDG-PET imaging may be a useful parameter for predicting patient outcome [32].

## *4.3 Clear Cell Chondrosarcoma*

Clear cell chondrosarcoma (CCCS) is rare, constituting approximately 1 to 2 percent of all chondrosarcomas. Patients are most commonly affected in the third to fifth decade of life with a two-fold predilection for men [21]. The lesion tends to be slow-growing and less aggressive, leading to improved prognosis when compared to high-grade conventional chondrosarcoma. Distant metastasis and dedifferentiation is rare, but has been reported [33]. Pathologic fracture may be the presenting symptom in 25 percent of cases [21]. The long tubular bones are affected in 85 to 90 percent of cases; in particular, the proximal femur and proximal humerus are involved in 55 to 60 percent, and 15 to 20 percent of cases, respectively. One key radiographic finding for clear cell chondrosarcoma is its predilection for the epiphysis of long bones. The importance of distinguishing CCCS from other benign entities often centered in the epiphysis, such as chondroblastoma and giant cell tumor (GCT), is important. Conservative excision and curettage frequently results in CCCS recurrence, and en bloc resection may be required [33].

Radiographs reveal a lucent lesion with a variable zone of transition. Typical chondroid matrix mineralization is identified in only 30 percent of cases. A well-defined sclerotic margin may also be identified [33]. Bony remodeling and expansion may be identified in approximately 30 percent of cases, with soft tissue extension being rare but present more frequently in lesions involving the axial skeleton [21]. Periosteal new bone formation is rare [33]. CT examination, like in conventional intramedullary chondrosarcoma, will help identify matrix mineralization, osseous destruction, and soft tissue extension, particularly in anatomically challenging locations such as the flat bones or vertebrae. [33].

MRI shows homogenous or heterogeneous low to intermediate signal on T1 sequences with heterogeneous high signal on T2-weighted sequences [21, 33].

Low signal on T2-weighted sequences has also been reported [21]. Areas of heterogeneity on MRI appear to correlate with mineralization, hemorrhage, and cystic changes. Post-contrast T1 images display a diffuse or heterogeneous pattern of enhancement, which is nonspecific and is also observed in benign chondroblastoma [33, 34].

As noted above, important differential considerations for an epiphyseal lesion such as CCCS include chondroblastoma and giant cell tumor. On MRI, chondroblastoma tends to have low to intermediate signal on T1 sequences and T2 sequences, but high T2 signal has been observed in cystic areas of chondroblastoma and giant cell tumor [33, 34]. Chondroblastoma affects a younger population (third and fourth decade), has a similar male predilection, and tends to be confined solely to the epiphysis with distinct sclerotic margins [21, 33, 34]. It is commonly found about the knee or proximal humerus; rarely, it is found in the hands and feet [35]. Chondroblastoma tends to have extensive peritumoral bone marrow edema (not common in CCCS) and surrounding soft tissue edema (occasionally seen in CCCS) [33, 34]. Definite differentiation of CCCS from chondroblastoma is difficult, but a diagnosis of CCCS may be implied when considering the patient's age, metaphyseal extension, and lack of bone marrow edema [33, 34].

Giant cell tumor, in contrast, is a lucent lesion that begins in the metaphysis and usually involves the epiphysis at the time of presentation (usually after skeletal maturity). These well-circumscribed lesions are characterized by the lack of a host response (such as a sclerotic margin or periosteal reaction) and the lack of internal matrix. Cortical breakthrough, an associated soft tissue mass, and internal low signal on MRI due to hemosiderin can also be seen [34, 36].

## *4.4 Juxtacortical Chondrosarcoma*

This is a rare lesion, accounting for about 4 percent of all chondrosarcomas [21] (Fig. 15.7). Due to its origin on the bone surface, it has also been termed periosteal or parosteal chondrosarcoma. Patients tend to be in their fourth or fifth decade and there is a slight male predilection. Patients typically report a palpable, painless slowly growing mass [21, 37]. Lesions tend to arise on the surface of long bones, with the most frequent site being the posterior distal femoral metaphysis or diaphysis. Juxtacortical chondrosarcoma can recur after excision, and dedifferentiation has been reported [37].

Radiographs display a characteristic round or oval soft tissue mass on the bone surface with a chondroid matrix. The underlying bone cortex is often thickened with a Codman triangle pattern of periosteal reaction [38]. As with other chondrosarcomas, CT can help better define the matrix mineralization, with the non-mineralized portion showing attenuation values less than that of muscle [21]. MRI displays a lesion with low heterogeneous signal on T1-weighted

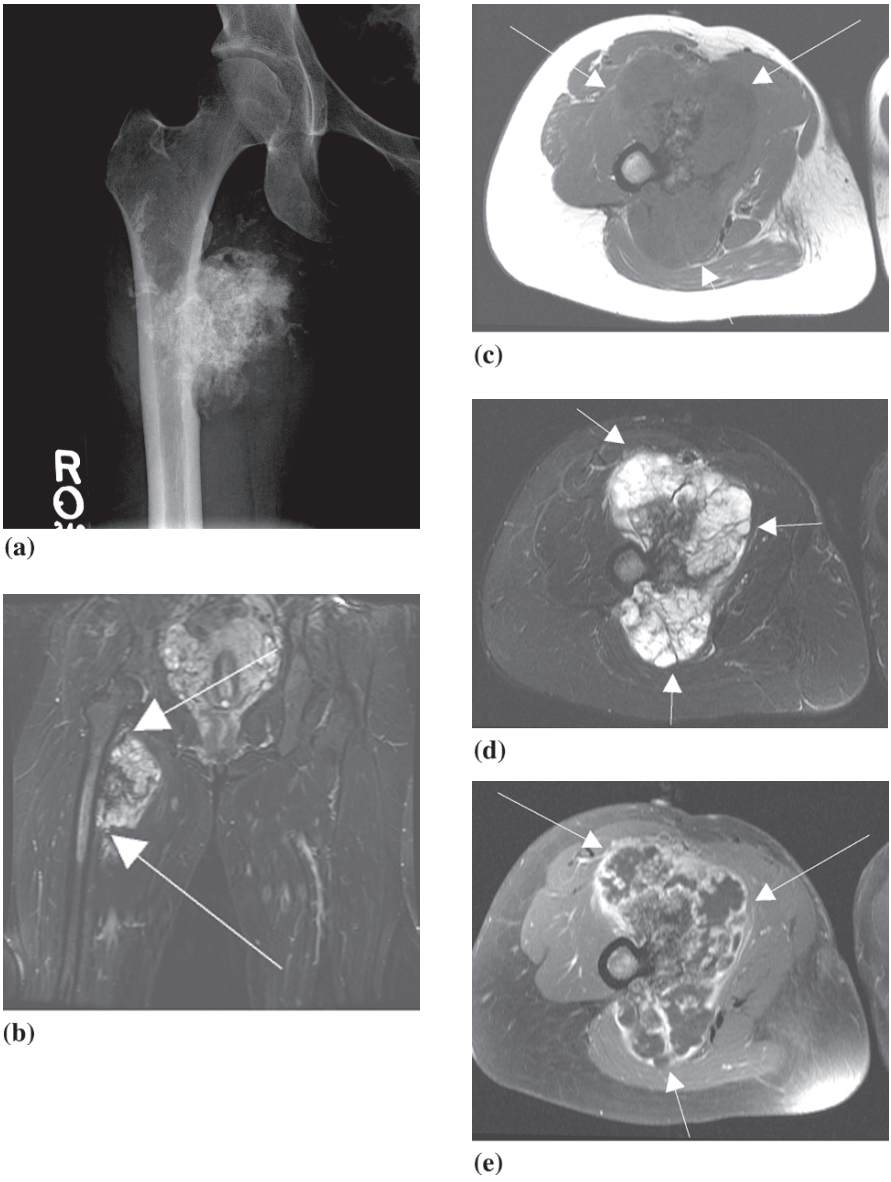


**Fig. 15.7** Low-grade juxtacortical chondrosarcoma in 34-year-old female. (**a**) Frontal radiograph displays a dense "arcs–and-rings" mineralization pattern associated with a partially calcified soft tissue mass. (**b**) Coronal STIR, (**c**) axial proton density, (**d**) axial STIR, and (**e**) axial T1 post-gadolinium fat saturation images show the T2 hyperintense cartilage within the lesion (best seen on the STIR image) and nodular peripheral and septal enhancement (best seen on the T1 post-contrast image). Note the excellent soft tissue contrast which permits evaluation of neurovascular structures for resection planning

images and heterogeneous high signal on T2-weighted images. The bone marrow is typically spared. Contrast-enhanced scans reveal peripheral and septal enhancement.

These imaging characteristics are nonspecific and the differential when approaching such a lesion includes a juxtacortical chondroma, parosteal osteosarcoma, and periosteal osteosarcoma. Chondromas occur three to four times more frequently, but can possess similar imaging characteristics including matrix calcification, intramedullary extension, bone edema, and irregular soft tissue margins [39]. Lesion size may be the only helpful characteristic in differentiating juxtacortical chondroma from juxtacortical chondrosarcoma; chondromas tend to be smaller, averaging 2 cm, while juxtacortical chondrosarcoma averages approximately 5 cm [21, 39]. Some have advocated that all lesions greater then 3 cm should, therefore, undergo wide surgical excision [39].

Differentiating juxtacortical chondrosarcoma from periosteal and parosteal osteosarcoma is also difficult. Periosteal osteosarcoma has a similar histologic appearance, but is usually present in younger patients (10 to 25 years) and is associated with periosteal reaction that occurs perpendicular to the cortex, which is uncommon in juxtacortical chondrosarcoma [40]. Parosteal osteosarcoma appears similar radiographically, except it usually displays a stalk of attachment to the cortex and does not contain chondroid tissue histologically.

## *4.5 Skeletal Myxoid Chondrosarcoma*

Morphologically distinct myxoid chondrosarcoma of the bone (skeletal myxoid chondrosarcoma) is not a well-established entity, but myxoid components are common in conventional intramedullary chondrosarcoma. It is well known that extraskeletal myxoid chondrosarcoma frequently possesses recurrent translocation t(9;22)(q22–31;q11–12), although this genetic abnormality has not been consistently detected in myxoid chondrosarcoma of the bone, suggesting that the soft tissue and intraosseus entities are distinct [41]. Due to the limited number of cases, few conclusions can be drawn about the tumor, but it appears to have a male predilection and is often found in the femur [21]. Although initially believed to be less aggressive, the tumor has been shown to have a high recurrence rate and often develops distant metastases [21, 41].

Radiographically, myxoid chondrosarcoma of the bone does not possess any unique imaging features. It appears aggressive with a lytic permeative pattern, endosteal scalloping, cortical destruction, bony expansion and an associated soft tissue mass [21, 41]. Matrix mineralization may be noted, often more easily detected with CT. CT or MRI can better define soft tissue extent and cortical destruction. MRI displays high signal on T2-weighted sequences with most tumors displaying a component of hemorrhage, especially involving the soft tissue component. Mild contrast enhancement is typical [21].

## 4.6 Mesenchymal Chondrosarcoma of Bone

Mesenchymal chondrosarcoma accounts for around 2 to 13 percent of chondrosarcoma of the bone [21]. It often presents like other malignant bone tumors, with pain and soft tissue swelling. Unlike other chondrosarcomas, it affects women and men equally and affects a younger population (third through fifth decades). In contrast to conventional chondrosarcoma, it most commonly involves the axial skeleton with the craniofacial region being most common (15 percent to 30 percent of cases). Other common sites include the femur, ribs, spine, pelvis, and humerus [21]. Prognosis is unpredictable, but overall survival is poor with a five-year survival rate of 42 to 55 percent, and 10-year survival rate under 30 percent. Distant metastases have been reported after resection [42-44]. Proliferative activity of the cells is being investigated for use as a prognostic factor [43]. Radical surgery is the primary treatment with adjuvant chemotherapy/radiation used pre-operatively or for recurrence and metastases [42, 44].

Radiographs typically display a nonspecific permeative pattern of bone destruction and ill-defined periosteal reaction. Extensive extraosseous components are common and, while not always prominent, an "arc-and-rings" chondroid calcification pattern is noted in up to 67 percent of cases. Most are centered within the medullary cavity, but 6 percent may be surface lesions [21, 42, 45].

CT is helpful in further characterizing the findings noted on plain radiographs. Aggressive bone destruction and an associated soft tissue mass are common. The calcification tends to be stippled, but may appear subtle or heavy on CT [42]. Tumors often have foci of low attenuation, and this is believed to represent necrosis [21].

MRI tends to display low to intermediate intensity on T1-weighted images and intermediate signal on T2-weighted images. Contrast-enhanced images are helpful with mesenchymal chondrosarcoma, as enhancement is often diffuse without the typical pattern of septal and peripheral enhancement seen in other forms of chondrosarcoma. Some may also display high flow serpentine vessels on MRI, a feature not seen in other chondrosarcomas [21, 42]. The features of intermediate T2 signal (lower than other chondrosarcomas) and more intense enhancement on MRI can suggest the diagnosis, although tissue diagnosis remains necessary. On histology, mesenchymal chondrosarcomas display a characteristic bimorphic appearance, virtually pathognomonic, with islands of differentiated cartilaginous tissue surrounded by highly cellular zones with plexiform vascular networks [42]. Nuclear imaging with thallium has been reported as a means of identifying metabolically active lesions, and as a screening method for metastasis [42].

## 4.7 Dedifferentiated Chondrosarcoma

Dedifferentiated chondrosarcoma, also known as spindle cell chondrosarcoma, represents approximately 9 percent to 10 percent of all chondrosarcomas [21]. Multiple theories exist as to how these types of tumors arise, the most popular being

that a high-grade non-cartilaginous component arises in a lower grade, long-standing chondrosarcoma. Patients tend to be older than in other forms of chondrosarcoma, averaging 60 years old, and there is no gender predilection. Most tend to present with pain or pathological fracture. A soft tissue mass is seen in around 55 to 87 percent of tumors [21, 46, 47]. Lesions often arise from conventional chondrosarcomas or enchondromas [48]. Locations mirror those of conventional chondrosarcoma, with an intramedullary location and most commonly involving the femur [47]. Case reports of a peripheral location in bone similar to juxtacortical chondrosarcoma have also been published [37]. The chondroid component tends to be sharply demarcated from the non-cartilaginous component, which is often (in descending order of frequency) osteosarcoma, fibrosarcoma, or malignant fibrous histiocytoma (MFH) [47, 49-51]. Radiographic appearance varies, based on the size of the non-cartilaginous component of the tumor. Lesions usually display the features of conventional chondrosarcoma as discussed previously, while the dedifferentiated components are associated with more aggressive bone lysis, cortical destruction, and absent chondroid matrix [49].

CT and MRI help to display the two components (chondroid and non-chondroid) involved in these tumors, referred to as tumor bimorphism. Overall, one review showed evidence of bimorphism in approximately 35 percent of radiographs, 48 percent of CT scans, and 33 percent of MR images [49]. The soft tissue mass and chondroid component may be missed by plain radiograph [49]. The extraosseous soft tissue component is more likely to harbor the high-grade neoplasm than the intraosseous component [21]. With contrast, most lesions display heterogeneous enhancement, with around 50 percent displaying a more diffuse, prominent enhancement pattern characteristic of dedifferentiation [49]. The high-grade non-cartilaginous component often has soft tissue attenuation on CT with variable enhancement. On MRI, an important finding is lower T2 signal intensity of the dedifferentiated component relative to the adjacent chondroid tissue [50, 52].

Recognition of dedifferentiation can provide important information whereby to discuss prognosis; dedifferentiated chondrosarcoma is associated with poor prognosis, an aggressive pattern, and the ability to metastasize [51]. The five-year survival is approximately 10.5 to 24 percent with a median survival of 13 months. Most demonstrate poor response to systemic chemotherapy [47, 51]. The association between the type of tumor in the dedifferentiated component and prognosis has not been well-defined, although metastasis at diagnosis and a higher percentage of dedifferentiated component in the lesion results in a poorer outcome [47].

Imaging may play its largest role in guiding biopsy in these patients. It is imperative that the dedifferentiated component is identified and targeted during biopsy to render an accurate diagnosis for treatment planning [50, 52]. Wide or radical surgical margins are mandatory for treatment; however, it is unclear whether radical resection improves long-term results [48].

# 5 Multiple Myeloma

## *5.1 Introduction*

Multiple myeloma is the most common primary skeletal malignancy, with approximately 14,000 new cases in the United States per year [53]. The median age at diagnosis is 65 years, with a higher incidence in men and African Americans [54]. The disorder is caused by a clonal proliferation of plasma cells. While the exact cause is not yet defined, many patients have been found to have an abnormal karyotype, and having a chromosome 13 deletion has been found to correlate with patient outcome [53, 54]. Clinically, the diagnosis is based on an elevated level of gamma globulin on serum protein electrophoresis, and the presence of at least 10 percent abnormal plasma cells in a bone marrow aspirate specimen [53, 54]. Assessment of tumor burden aids treatment planning and prognosis determination; this assessment can include both imaging and measurement of serum markers such as Serum β2-Microglobulin, C-reactive protein, and lactose dehydrogenase (LDH).

The radiographic findings of multiple myeloma range from subtle to prominent. The classic descriptors of multiple myeloma on radiographs are diffuse osteoporosis and multiple "punched out" lucent lesions. The lucent lesions of multiple myeloma are caused by the increased osteoclastic cell response induced by the invasion of myelomatous cells into bone marrow [54]. Importantly, approximately 50 percent bone destruction must occur before a lucent lesion is visible on radiographs [54].

## *5.2 Myeloma Subtypes*

Imaging plays an important role in the diagnosis and differentiation of many of the subtypes of monoclonal gammopathy, including monoclonal gammopathy of undetermined significance (MGUS), asymptomatic myeloma, and symptomatic multiple myeloma. Additional subtypes also include solitary plasmacytoma and extraskeletal plasmacytoma.

The diagnosis of MGUS is based on mild elevation of gamma globulin on serum protein electrophoresis (SPEP). The patients should be asymptomatic and have no other clinical findings of multiple myeloma. These patients were once thought to have no osseous involvement [55], although some reports suggest that this may not be entirely accurate. A small series of 37 patients with MGUS revealed MRI abnormalities in seven patients, of whom four had diffuse patchy spinal MRI marrow signal abnormalities and three displayed focal abnormalities [56]. The patients with abnormal MRI findings progressed to require treatment for myeloma faster than those without MRI abnormalities, suggesting that the subset of MGUS patients with abnormal marrow signal on MRI may require closer follow-up. MGUS has a

**Table 15.2** Durie/Salmon PLUS Staging System for Multiple Myeloma. Staging of multiple myeloma using imaging characteristics. The distinction between substages A and B is based on serum creatinine and the presence or absence of extramedullary disease (EMD): Substage A is serum creatinine < 2.0 mg/dL and no EMD. Substage B is serum creatinine > 2.0 mg/dL and/or EMD. *Adapted from Durie, et al. [55].*

| Classification | MRI and/or FDG-PET |
|---|---|
| MGUS | All negative |
| Stage IA (Smoldering or Indolent) | Single Plasmacytoma or Limited Disease on Imaging |
| Multiple Myeloma | |
| Stage IB | < 5 Focal Lesions, Mild Diffuse Disease |
| Stage IIA/B | 5-20 Focal Lesions, Moderate Diffuse Disease |
| Stage IIIA/B | >20 Focal Lesions, Severe Diffuse Disease |

risk of progression to multiple myeloma and other entities such amyloidosis, macroglobulinemia, leukemia, and lymphoma [53].

Asymptomatic myeloma, also known as indolent or smoldering myeloma, has slightly higher levels of gamma globulin on SPEP, as well as other laboratory abnormalities, but patients are still asymptomatic. Newly published consensus guidelines state that these patients most commonly have no imaging abnormalities, although a subset will have one lesion detected on imaging [53].

Symptomatic myeloma accounts for the majority of multiple myeloma cases and includes several subtypes such as classic, generalized, osteosclerotic and leukemic [53]. Imaging plays the largest role with symptomatic myeloma and has now been incorporated into the recently updated Durie/Salmon PLUS staging system [55, 57] (see Table 15.2). For purposes of the staging system, moderate diffuse spine involvement was defined as diffuse marrow abnormality on T1-weighted sequences with signal intensity of vertebral marrow brighter than the adjacent intervertebral disks, and severe diffuse spine disease was defined as diffuse marrow abnormality on T1-weighted sequences with signal intensity of vertebral marrow lower than or equal to that in the adjacent intervertebral disks [55].

## *5.3 Imaging in Multiple Myeloma*

The current standard approach in patients with multiple myeloma relies on the skeletal survey, which is abnormal in 80 percent to 90 percent of newly diagnosed patients, and may be the only test needed for staging purposes, based on the number of lesions [53]. This usually consists of standard AP and lateral radiographs of the skull and spine, with additional anteroposterior radiographs of the ribs, pelvis and all long bones. Newer techniques involve the use of whole-body imaging C-arms [58]. Targeted radiographs in regions that are difficult to assess (including the ribs and scapula) may be ordered based on clinical suspicion or questionable abnormalities viewed on survey [53]. Skeletal survey displays the most abnormalities in the

classic and leukemic subtype of symptomatic myeloma, while the generalized subtype displays only diffuse osteopenia with no focal lytic lesions. The osteosclerotic subtype displays sclerotic lesions and is often seen in the POEMS syndrome (polyneuropathy, organomegaly, endocrine disorders, monoclonal gammopathy and skin changes). Some myeloma patients may display both lytic and sclerotic lesions without any of the additional findings associated with POEMS syndrome [53]. It is important to remember that, while the majority of lesions associated with multiple myeloma are lytic, sclerotic subtypes exist and should be considered when interpreting radiographs in patients with suspected or known multiple myeloma.

MRI has been established as an appropriate imaging modality in the diagnosis and follow-up of multiple myeloma, although no standard imaging protocols (including standards of anatomic coverage) have been established (Figs. 15.8, 15.9). A recent review on myeloma noted that no definitive conclusion can be drawn based on the available evidence and, instead, recommended inclusion of the entire skeleton or to broaden coverage as much as could be tolerated by the patient or the constraints of resources at one's institution [53]. Several large reviews on myeloma have suggested the use of MRI to evaluate the skull, entire spine and pelvis [54], or performing whole-body MRI examination [58, 59] (Fig. 15.10). If staging with whole-body MRI indicates stage III disease, no other imaging may be needed. In contrast, findings suggestive of stage I or II disease may indicate a need for additional imaging to prevent understaging in up to 10 percent of patients [58, 60]. A recent review showed whole-body MRI and skeletal survey to be discordant in 24 percent of cases, with 19 percent of cases having false negative skeletal surveys and stage III disease by spinal MRI [61]. The use of gadolinium is also controversial, with some employing the intravenous contrast on initial scans and others recommending its use only on follow-up scans, suggesting that enhancing areas are likely to harbor persistent disease [53, 54].

Before an MRI-based diagnosis is made it is important to understand the spectrum of normal marrow appearance, based on patient age. On T1-weighted images, fatty marrow is hyperintense and cellular marrow is hypointense relative to the intensity of skeletal muscles. With age, there is a replacement of cellular red marrow to a more T1 hyperintense fatty marrow. Caution must be used when identifying diffuse T1 hypointense areas with hyperintense nonuniform or band-like end plate changes as abnormal, because these findings can be normally seen in over 85 percent of patients aged 40 to 50 years [54]. Accurately differentiating myeloma from other marrow infiltration processes or metastasis is important. Iatrogenic processes are particularly important to consider in myeloma patients; for example, marrow changes have been noted in patients with primary musculoskeletal malignancies receiving GCSF. One small study found that red marrow conversion from treatment resulted in low signal on T1 and mildly increased signal on T2 images, when compared to normal yellow marrow, findings that can also be found in myeloma and tumor metastasis to the marrow. The pelvis and proximal long bones were noted to be affected most frequently [62].

MRI may be used to assess tumor burden, with low burden usually being associated with no MRI abnormalities and high burden associated with diffuse hypointensity on

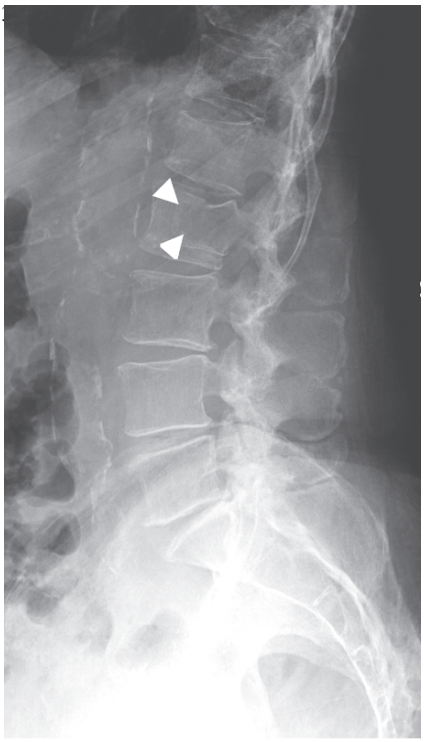

(a)

(b)

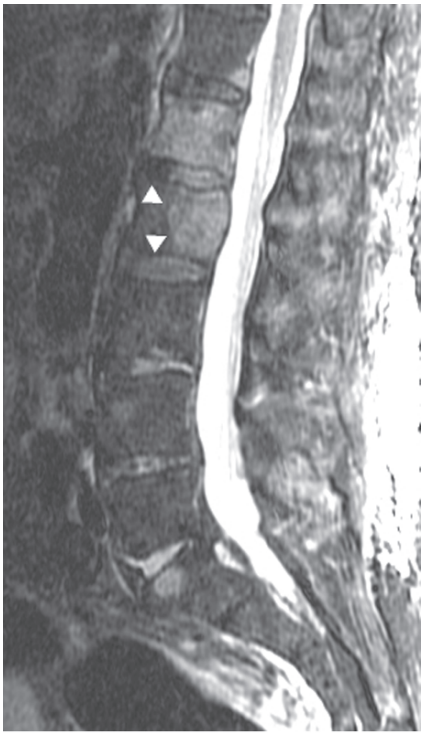

(c)

T1 sequences, high signal on fluid sensitive sequences, and enhancement with gadolinium. Marrow signal may be homogeneous or heterogeneous. Numerous studies have shown that the pattern of diffuse marrow involvement, as detected by MRI, correlates with increased marrow cellularity, increased plasmacytosis, anemia and overall poorer survival when compared to patients with a normal MRI pattern [54, 63]. Lecouvet, et al. reported 37 percent 60-month survival rates in stage III patients with diffuse MRI abnormalities, compared to 70 percent in patients with a normal MRI pattern. Prior studies in early stage myeloma patients have also found a diffuse MRI pattern to be associated with early progression [63].

Spinal fractures are commonly associated with multiple myeloma, and are seen in approximately 55 percent to 70 percent of patients. In one review of spinal fractures imaged with MRI, 80 percent of single fractures were associated with a focal lesion, although only 46 percent of fracture sites in patients with multiple fractures were associated with a focal lesion. These results suggest that fractures can occur at sites that appear normal on MR images. Additionally, patients with diffuse disease on MR images have a shorter fracture-free interval than those without diffuse disease [54]. Compression fractures without associated edema on MRI have been reported [64]. In addition to morphologic and signal characteristic criteria, in-phase and opposed-phase MRI may help accurately distinguish spinal fractures due to benign versus malignant causes [65]. Multiple studies have demonstrated the efficacy of vertebroplasty in treatment of myeloma-related fractures [64].

Recent work has evaluated the use of CT in diagnosis of myeloma, and in predicting the risk of impending spinal fractures. It is generally accepted that CT is superior to conventional radiographs in identifying lytic lesions in certain areas of the body, including the ribs, skull, and axial skeleton, and recent reports have found that whole-body CT detects more focal lesions and can lead to changes in staging [53, 54]. However, replacement of the conventional skeletal series with whole-body CT has not been universally accepted due to increased radiation exposure. Low dose protocols have been developed and found to be successful in diagnosis and identifying lesions at high risk for fracture [66]. CT can also be used to guide biopsy for lesions defined by MRI, as larger gauge needles are difficult to use in the MRI environment. Targeted biopsies can increase yield and improve detection of cytologic and cytogenetic abnormalities, resulting in the alteration of a patient's treatment plan [54].

Bone scintigraphy with $^{99m}$Tc-MDP generally does not play a significant role in staging or diagnosis of myeloma, as the modality relies on osteoblastic and not osteoclastic activity; as a result, myelomatous lesions do not demonstrate increased

**Fig. 15.8** Comparison of radiographs, CT and MRI in the imaging of the lumbar spine in an 88-year-old male with multiple myeloma. (**a**) Lateral radiograph, (**b**) sagittal CT reformat, (**c**) and sagittal STIR MRI demonstrate varying sensitivity for detection of individual lesions. Note the different appearance of the dominant L2 lytic lesion (arrowheads). The MR images reveal numerous lesions that are subtle or occult on the other modalities

**(a)**

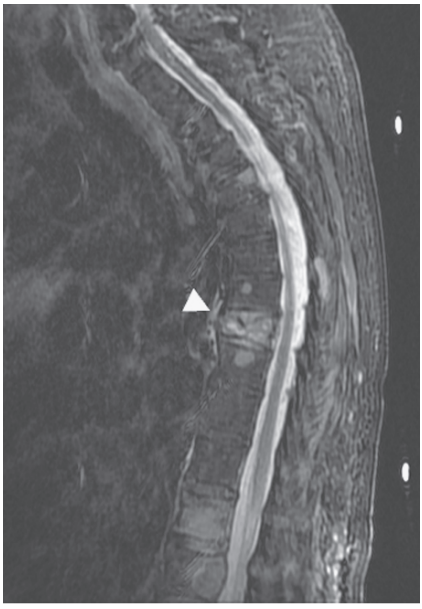

**(b)**

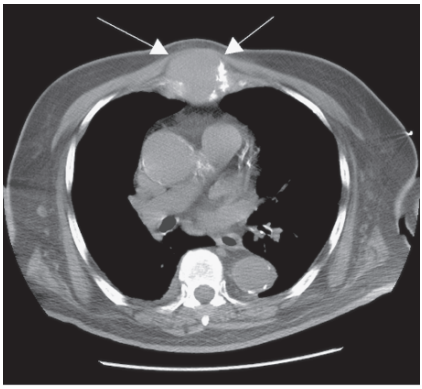

**(c)**

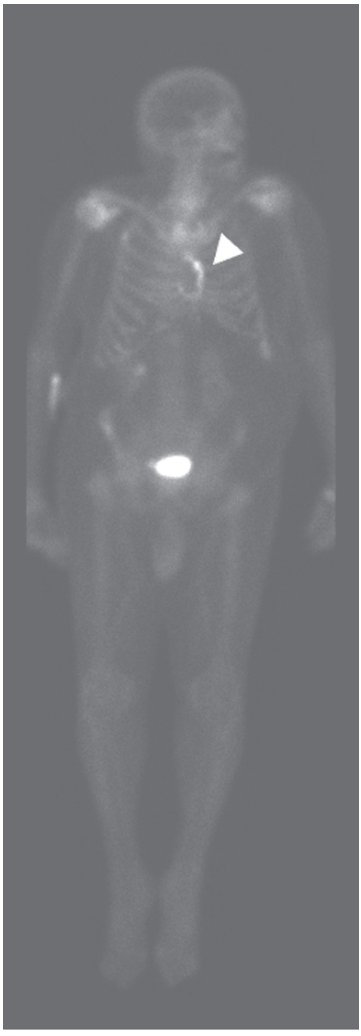

**(d)**

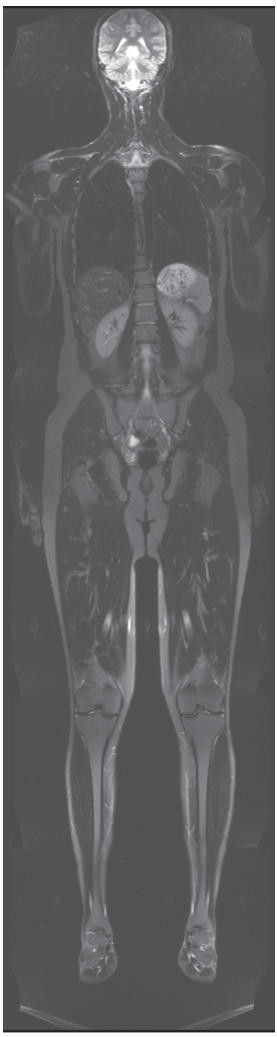

(a)

(b)

**Fig. 15.10** Normal whole-body STIR MRI scans from newly diagnosed 60-year-old man with multiple myeloma. Images courtesy of Dr. Michael Mulligan. Reprinted from [58]

**Fig. 15.9** (**a**) Sagittal T1 and (**b**) sagittal STIR MR images of the thoracic spine, (**c**) axial CT image of the chest including the sternum, and (**d**) bone scintigraphy in a patient with multiple myeloma. Sagittal T1 MRI image shows multiple lesions replacing the high intensity marrow, consistent with imaging Stage II myeloma. STIR MR image shows multiple hyperintense lesions that contrast with the low signal marrow fat, as well as a compression fracture (white arrowhead). CT demonstrates a sternal lesion (arrow) that is evident as a region of a photopenia with surrounding uptake on the bone scan (white arrowhead)

uptake on scintigraphy. Multiple studies have confirmed that bone scans tend to underestimate the extent of disease [54]. $^{67}$Galium citrate, $^{99}$Tc MIBI and, $^{201}$Tl chloride have all been investigated as potential agents for use in myeloma with promising results, although none have been integrated into standard care for myeloma patients. Focal MIBI uptake appears to be better associated with active myeloma than diffuse uptake [67].

## *5.4 The Role of FDG-PET*

FDG-PET appears to be an acceptable complementary imaging modality to stage and monitor treatment (Fig. 15.11). Mixed results have been obtained when comparing PET/CT to other imaging modalities, including skeletal survey, CT, and MRI. Breyer, et al. used SUV values of greater then 2.5 and found that PET/CT identified approximately 104 (14 soft tissue and 90 osseous lesions), of which 57 (55 percent) were new or previously undetected. In this series, conventional skeletal series missed 56/57 of the lesions, while CT failed to detect nine of these sites. PET had a low sensitivity in this study, as 133 sites felt to represent myeloma were identified by the other modalities (radiograph, CT or MRI) and not detected on PET. Many of these were missed due to their small size, as PET has limited spatial resolution and suffers from volume averaging effects [68]. However, Nanni et al. showed PET/CT to be more sensitive then whole-body X-ray by identifying lesions below the contrast resolution of X-ray and those with less then 50 percent bone resorption [69]. Comparing PET to MRI has also been mixed: while PET can detect lesions outside of MRI's field of view (particularly when whole-body MRI is not available), there is diminished sensitivity in identifying diffuse spinal disease evident on MRI [68, 69]. PET is also subject to false positives caused by infection, inflammation, post-surgical or radiation changes, and hemangiomas [68, 69].

Detection of previously occult lesions on PET scan can upstage patients [68, 70]. When interpreting PET scans, an SUV value threshold of 2.5 may be inappropriate, as smaller myeloma lesions have been evaluated in retrospect to be FDG avid with values below the threshold of 2.5. This has prompted some to suggest that any FDG uptake (regardless of SUV value) in lesions smaller then 5 mm should be viewed with suspicion as an additional focus of disease [58]. At least one report suggests that following treatment, a decrease in uptake values on FDG-PET has predicted clinical outcome [70].

Future work with PET or PET/CT will likely focus on using imaging to help determine which lesions are "active," and whether this finding can be incorporated into staging systems. The combination of PET/CT may also enable simultaneous evaluation of lesions with two distinct radiologic methods. Some institutions have recommended use of FDG-PET routinely in patients with non-secretory myeloma, solitary plasmacytoma of the bone, or extramedullary plasmacytoma and consider it as a potential modality for future use in routine radiologic follow-up in myeloma patients to examine disease response [58].

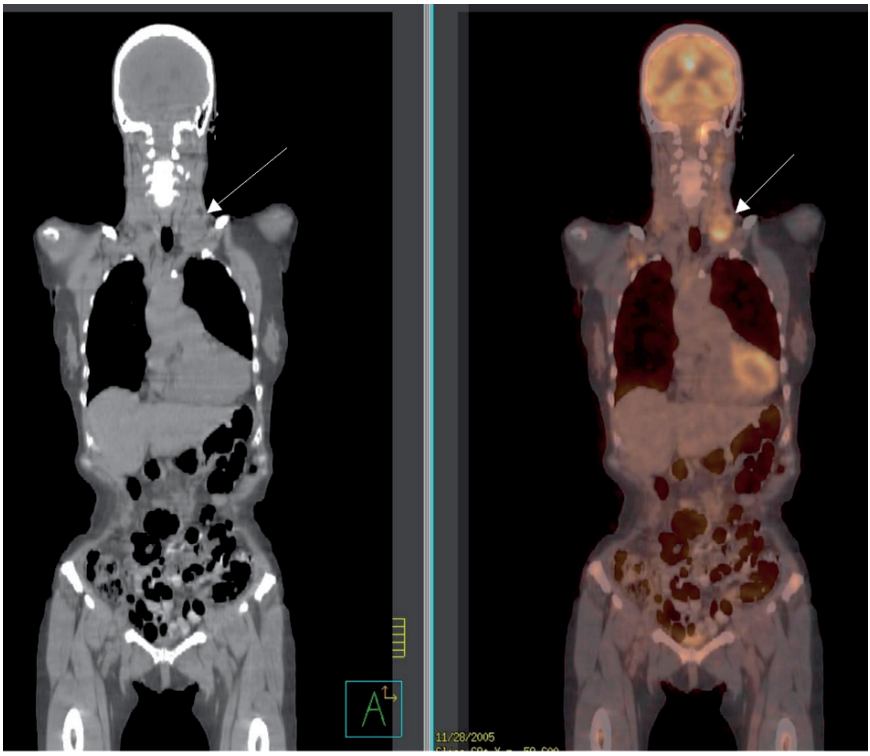


**(a)**

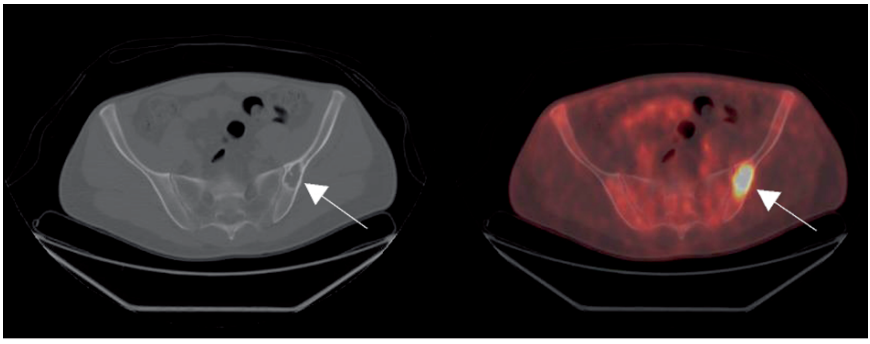

**(b)**

**Fig. 15.11** PET/CT in multiple myeloma. (**a**) Coronal CT and fused PET-CT images in 71-year-old female with myeloma and new neck mass. FDG avid focus (SUV=3.5) is noted within enlarged left neck lymph nodes (arrows), representing a biopsy proven extramedullary myeloma recurrence. Images courtesy of Dr. Michael Mulligan. Reprinted from (58). (**b**) CT and fused PET/CT axial images in 42-year-old male with biopsy proven lytic solitary plasmacytoma (arrows) with standardized uptake value (SUV) of 10

### 5.5 Solitary Plasmacytoma and Extramedullary Plasmacytoma

Solitary plasmacytoma accounts for 2 percent to 5 percent of most cases of myeloma [53, 54]. The most common site of involvement is the spine. Flat and long bone lesions can have almost any radiographic appearance, from benign-appearing to aggressive [53]. Patients present with bone pain, and treatment consists of local radiation, although patients are prone to developing symptomatic multiple myeloma within a short time of diagnosis. Radiologic work-up of these lesions starts with the classic skeletal survey. MRI has been suggested as an adjunctive imaging procedure, as it displays abnormalities not picked up on original survey in one-third of patients and helps better define soft tissue extent for radiation therapy [71]. Lesions greater than 5 cm have been associated with poorer prognosis [53].

Extramedullary plasmacytoma accounts for approximately 3 percent of myeloma cases and has a 3 to 1 male predominance. Most cases are found within the head/neck region, notably involving the paranasal sinuses and oropharynx [53]. Imaging work-up for these lesions is similar to solitary plasmacytoma, with the adjunctive role of MRI and FDG-PET not firmly established [53]. Treatment is radiation therapy or surgical excision.

### 5.6 Multiple Myeloma: Follow-up

Acceptable protocols for radiologic follow-up in myeloma patients are not well established. Some authors believe that routine radiological (in addition to serologic) follow-up is not indicated in myeloma, while others employ MRI to help determine treatment response. Defining an acceptable standard imaging follow-up regimen is still necessary in asymptomatic patients; changes in a patient's symptoms is obviously an indication for re-assessment [58].

## 6 Metastasis

### 6.1 Introduction

Metastases represent the most common type of malignant bone lesion, accounting for approximately 70 percent of bone tumors, and should always be considered in the differential diagnosis of a skeletal lesion, particularly in older patients. Bone metastasis is 25 times more common than primary bone tumors [72]. Following the lungs and liver, the skeletal system is the third most common location of distant metastases. The most common sources of osseous metastases include breast, prostate, lung, colon, stomach, rectum, uterus, bladder, renal and thyroid primary malignancies; of these, breast and prostate cancer represent the most common primary

sites [73]. Clinically, patients can present with severe bone pain, bone tenderness, soft tissue mass, pathologic fracture and spinal cord compression, all of which reduce quality of life and worsen prognosis. Life-threatening hypercalcemia is another possible effect of bone metastasis [73]. Radiographs, scintigraphy, CT and MRI are all currently utilized for detection and monitoring of metastases, with PET and whole-body MRI providing promising diagnostic potential. Despite this variety of modalities, metastases present a diagnostic challenge for radiologists due to the wide variability in radiologic appearance and the difficulty in measuring response to treatment.

## *6.2 Mechanisms and Radiographic Appearance*

Metastatic disease of the skeleton can arise from direct extension, hematogenous or lymphatic dissemination, or intraspinal spread of tumor. Bone represents an excellent site for metastatic tumor cells, due to high blood flow (particularly in red marrow), adhesive molecules on tumor cells that can induce production of angiogenic and resorptive factors when bound to bone marrow stromal cells or bone matrix, and immobilized growth factors that are present to support ongoing bone remodeling and resorption [73]. Direct extension, such as a lung cancer invading the ribs, typically involves a soft tissue mass and osseous destruction. Lymphatic spread is particularly relevant for pelvic cancers such as prostate, bladder or gynecologic cancers, where spread to local lymph nodes can then directly invade adjacent structures. Hematogenous spread can occur via arterial or venous routes. Intraspinal spread can occur when an intracranial neoplasm gains access to cerebrospinal fluid, allowing drop metastases to form within the spinal canal with secondary invasion of the vertebrae.

The typical classification of bone metastasis distinguishes between osteolytic (lucent) and osteoblastic (sclerotic) lesions. These broad categories represent the two extremes of abnormal bone metabolism and remodeling that occurs in the presence of an osseous metastasis [73]. Osseous structures respond to neoplastic infiltration with varying degrees of bone resorption and formation. Resorption is thought to occur by osteoclast activating factors released by tumor cells, among other mechanisms. The mechanism of osteoblastic metastases is less understood. There is evidence, however, of a “vicious cycle” in breast and prostate cancer metastases in which tumor cells promote proliferation of osteoclasts and vice-versa [73].

The distribution of the radiographic appearance of metastatic lesions includes osteolytic (75 percent of metastases), osteosclerotic (15 percent) and mixed lytic/sclerotic (10 percent) (see Table 15.3). Lytic metastases can arise from the breast, thyroid, kidney, lung, breast, gastrointestinal tract, adrenal gland, uterus, Ewing’s sarcoma, squamous cell carcinoma and pheochromocytoma. Bubbly expansile lytic metastases are seen in renal and thyroid metastases. Sclerotic lesions are typically seen with prostate cancer, as well as carcinoid tumors, medulloblastoma and

**Table 15.3** Common Appearance of Skeletal Metastases. Note that the table presents the most common appearance of each primary tumor type, although any individual lesion can have a different appearance, particularly following treatment

| Primary Tumor Type | Imaging Appearance |
|---|---|
| Breast | Lucent or Mixed |
| Lung | Lucent or Mixed *(Occasionally Sclerotic with Small Cell Carcinoma and Adenocarcinoma)* |
| Prostate | Sclerotic |
| Kidney | Lucent, Expansile |
| Thyroid | Lucent, Expansile |
| Melanoma | Lucent, often with soft tissue mass |
| Bladder | Lucent |
| Esophagus | Lucent |
| Stomach | Lucent (Sclerotic in Mucinous subtypes) |
| Colon | Lucent or Mixed (Sclerotic in Mucinous subtypes) |
| Pancreatic | Lucent |
| Uterus/Cervix | Lucent |
| Ovarian | Lucent, Mixed, or Sclerotic |
| Neuroblastoma | Lucent, Permeative |
| Retinoblastoma | Lucent, Permeative |

osteosarcoma. Mixed lytic/sclerotic lesions can be seen in almost any metastasis, including from breast, lung, cervical, ovarian, colon and testicular tumors.

Metastases have a predilection for the red marrow-rich axial skeleton, particularly the lumbar and thoracic vertebral bodies, pelvic bones, sternum and ribs. The vertebrae house 75 percent of the body's bone marrow and are highly vascular, making them especially susceptible to metastatic spread. Vertebral metastases most commonly arise from carcinomas of the lung, breast, and prostate, as well as lymphoma and myeloma. Sclerosis of a vertebral body, such as an "ivory vertebrae" (increased density of the entire body) or partial sclerosis, can be seen most commonly in prostate metastases, as well as lymphoma, myeloma, and Paget's disease. Spinal metastases may also present as a malignant vertebral body compression fracture; differential possibilities would include both malignant (myeloma) and benign (osteoporosis) etiologies. Characteristics more commonly seen in metastases than in these other entities include compression of an upper level thoracic vertebrae, associated soft tissue mass, and destruction of the pedicle, usually by direct extension from the vertebral body. Definitive diagnosis can be made by biopsy.

In the appendicular skeleton metastatic disease is most commonly proximal in location; it is rare to have metastatic disease distal to the elbow or knee. Notable exceptions are bronchogenic carcinoma and breast cancer, which can present with widespread skeletal metastases and together account for 50 percent of metastases distal to the elbows and knees. Relatively common locations for metastases are the proximal metaphyses of the humerus or femur, usually presenting as a medullary

lesion with later involvement of the cortex. These lesions usually do not have a significant soft tissue mass or periosteal reaction, in contradistinction to primary bone tumors. In long tubular bones, pathologic fracture can occur once more than 50 percent of the cortical thickness is destroyed.

## *6.3 Imaging Modalities*

Each imaging modality confers a specific subset of information that adds to the diagnostic query. Plain radiography and CT can demonstrate bone structure, CT and MRI visualize the tumor and bone marrow, bone scanning and SPECT can reveal osteoblastic metabolism, and PET can visualize tumor metabolism. MRI and PET can potentially detect early bone marrow changes, before structural changes are visible.

*Radiographs:* On radiographs, the appearance of metastases is highly variable, taking on any pattern of bony destruction (geographic, moth-eaten, permeative), with poorly or well-defined margins. Lesions can be lytic, sclerotic, or mixed lytic/sclerotic. Approximately 30 percent to 50 percent of normal bone mineral must be lost before a bone metastasis becomes visible on a plain radiograph, so metastases may remain occult for up to three to six months [72]. As most metastases spread hematogenously, tumor emboli tend to lodge in the marrow, with only later involvement of the cortex.

Differentiating metastases from primary bone tumors, infection, or metabolic lesions can be very challenging due to variable radiologic characteristics. In general, multiple lesions are more suggestive of metastases, though solitary metastases can occur (particularly with renal and thyroid metastases), and it can be difficult to differentiate solitary metastases from primary bone tumors. When multiple, metastatic lesions are usually variable in size, in contrast to multiple myeloma lesions which tend towards uniformity. Periosteal reaction and soft tissue mass are usually limited, in contrast to primary bone tumors. Additionally, metastatic lesions tend to be smaller, averaging 2 to 4 cm in diameter. Cortical metastases, which usually affect the femur, can be seen with bronchogenic carcinoma, melanoma, and cancers of the bladder and kidney.

Radiographically, a lytic lesion that is responding to chemotherapy or radiation therapy can develop peripheral sclerosis that moves centrally, with eventual resolution of the sclerotic area. Healing mixed lytic/sclerotic lesions become progressively more sclerotic. Meanwhile, lesion expansion or new zones of lysis usually indicate progression of disease. New areas of sclerosis can signify disease progression or healing of a previously unrecognized lesion.

*Bone scintigraphy:* Bone scintigraphy is the most commonly used modality in screening for metastases, with an approximate sensitivity of 62 percent to 100 percent, and specificity of 78 percent to 100 percent [74]. Bone scintigraphy is a useful screening tool as it can provide rapid whole-body images at a reasonable cost. Most commonly, metastases are seen as areas of increased tracer uptake (“hot spots”),

which reflects hyperemia, reactive repair, and new bone formation at the periphery of the lesion. Both lytic and sclerotic lesions tend to have increased tracer uptake. When the bony destruction is extensive, an area of decreased tracer uptake ("cold spot") can be seen. In challenging areas, such as the thoracolumbar spine and pelvis, tomographic information available using SPECT (single photon emission computed tomography) can be used to further define the anatomy.

Diffuse uptake by the axial skeleton, referred to as a "superscan," can be seen with diffuse prostate or breast metastases, and can be easily mistaken as normal because of the uniform increase in uptake. This pattern can be identified by the lack of tracer uptake in the genitourinary system and distal appendicular skeleton. Isolated foci of increased uptake (particularly involving the ribs or joints) in a patient with a known primary malignancy are usually benign lesions due to degenerative changes or old fractures.

Limitations of skeletal scintigraphy include the broad list of differential possibilities for a focus of increased radiopharmaceutical uptake. A wide variety of neoplastic, infectious, inflammatory, and traumatic etiologies can lead to a false positive scan. Metastatic lesions that do not have aggressive new bone formation or are rapidly expanding, may not demonstrate increased uptake, resulting in a false negative. Correlation with radiographs or CT, as necessary, can increase specificity of bone scintigraphy up to 95 percent [72].

A specialized type of scintigraphy – bone marrow scintigraphy – uses technetium-99 labeled monoclonal antibodies such as the NCA095 antibody to detect early bone marrow infiltration. In particular, bone marrow scintigraphy has been shown to be superior to conventional bone scintigraphy for certain tumor subtypes, such as small cell lung cancer and breast cancer with osteolytic metastases [72].

During therapy, tracer uptake on sequential scans cannot reliably be correlated with tumor behavior. A lesion may demonstrate increased uptake due to either disease progression or tumor healing. In the first three months post-therapy, 75 percent of metastases have increased tracer uptake, dubbed the "flare phenomenon," which subsequently subsides by six months post-therapy. Similarly, decreased tracer uptake may be due to healing or, less commonly, to advanced osseous destruction. Rather, the presence of new lesions is a more accurate indicator of disease progression. Again, correlation with the clinical picture and radiographic pattern are essential.

*Computed Tomography (CT):* CT is more sensitive than radiographs for detecting subtle osseous destruction, as well as an associated soft tissue mass. The sensitivity of CT ranges from 71 percent to 100 percent, and it is particularly useful in cases of a positive bone scan and equivocal radiographs. While cortical destruction and large lytic lesions are easily visualized on CT, subtle marrow lesions may be difficult to identify prospectively without physiologic information that can be obtained on bone scintigraphy or PET scan. CT findings suggestive of metastases include lytic lesions with associated cortical and trabecular destruction and high attenuation areas of soft tissue density within the predominantly low attenuation fatty marrow. Like radiographs, sclerosis usually suggests response to tumor, while progressive lysis can indicate disease progression. It is particularly important to examine the

entire imaged skeleton using display parameters optimized for visualizing bone ("bone windows") and multiple plane reformats.

*Magnetic Resonance (MRI):* MRI has a diagnostic sensitivity of 82 percent to 100 percent and specificity of 73 to 100 percent for bony metastases, and it is particularly sensitive in detecting bone marrow lesions. A number of recent studies have shown that MRI detects marrow changes even earlier than bone scintigraphy [72]. Metastases in the bone marrow lead to a longer T1 relaxation time (low T1 signal) due to edema and displacement of the marrow fat. Variable changes in the T2 relaxation time are seen, but lytic tumors tend towards high T2 signal, while sclerotic tumors have a low T2 signal. Solid, cell-rich tumors have intermediate T2 signal. Adding T2-weighted sequences with fat suppression results in suppression of the normal bone marrow and excellent contrast between the lesion and normal tissue. Phase shifted gradient echo imaging is very sensitive for detection of metastases. Gadolinium enhancement does not necessarily help with detection of metastases, although it can help delineate tumor extent and differentiate tumor necrosis from viable tumor.

It can be challenging to differentiate metastases from reconversion of hematopoietic bone marrow, which also results in low T1 and high T2 signal. Reconversion represents change from yellow marrow (predominantly fat) to red marrow (more cellular), and usually follows a predictable pattern from proximal to distal. A basic rule-of-thumb is that red marrow still has higher signal than muscle on T1-weighted images, in contrast to marrow-replacing neoplastic processes. Schweitzer et al. described a characteristic rim of T2 hyperintensity (edema) around a low signal intensity metastatic lesion, dubbed the "halo sign" [75]. Benign lesions have more of a "bull's eye" appearance with central T1 hyperintensity surrounded by a T1 hypointense lesion [75]. Gradient echo sequences are also useful in detecting normal hematopoietic bone marrow [72].

Another common diagnostic dilemma is differentiating pathologic vertebral body fractures from osteoporotic fractures. In general, the following findings are more characteristic of pathologic fractures: convex posterior contour of the posterior cortex of the vertebral body, abnormal signal in the pedicle or vertebral arch, associated soft tissue mass, normal signal in the adjacent disc, restricted diffusion on diffusion-weighted imaging and diffuse low T1 signal with corresponding increase in T2 signal intensity [72, 76].

Due to its high sensitivity for metastatic detection and ability to detect bone marrow disease earlier than bone scintigraphy, MRI has been proposed as a screening modality. Whole-body MRI (WBMRI) is a promising new staging method that can evaluate for both bony and parenchymal lesions while decreasing the time and expense involved in having multiple staging exams using several different modalities. In the past, WBMRI was technologically infeasible due to limited field of view, coil limitations, and unreasonably long exam times. Recent advances, including a whole-body coil system, new table concepts, and ultra-fast data acquisition have enabled researchers to attain high resolution images of the whole body within 14 minutes. Lauenstein et al. compared staging work-up in 51 patients using WBMRI

versus a multimodality approach employing bone scintigraphy, CT and MRI. WBMRI was able to detect all cerebral, pulmonary and hepatic metastases greater than 6 mm, resulting in sensitivity and specificity of 100 percent. Mean scan time was only 14.5 minutes. Tiny lung nodules that were missed by MRI did not change overall management [77].

There is limited data comparing WBMRI and PET/CT for detection of osseous metastases, although reported sensitivities range between 80 percent to 100 percent for both modalities, and there is evidence of overall concordance of 93 percent between the two modalities [72]. In a recent prospective study, Schmidt et al. compared WBMRI (using 32 channel parallel imaging) to PET/CT for the detection of bone metastases in 30 patients with a known primary tumor and suspected metastases. WBMRI had a sensitivity of 94 percent and specificity of 76 percent, while PET/CT had a sensitivity of 78 percent and specificity of 80 percent; at least part of this difference in performance is attributable to increased sensitivity for small lesions, with a minimum size threshold of 2 mm for WBMRI and 5 mm for PET/CT [78]. These results suggest that WBMRI may have a slightly superior diagnostic accuracy to PET/CT for metastatic screening, without exposing the patient to ionizing radiation [78]. Continued research in this modality should further define its performance and increase implementation at a broader range of centers.

*Positron Emission Tomography (PET):* The use of PET in the evaluation of malignancy has continued to increase, though its sensitivity in evaluating for bone metastases is not well established. FDG-PET has a sensitivity ranging from 62 percent to 100 percent, with a specificity from 96 percent to 100 percent [74]. When compared to bone scintigraphy, PET has a similar sensitivity through poorer specificity in detecting breast and lung metastases. PET is less sensitive in detecting prostate metastases, due either to the decreased metabolic activity of prostate metastases or the increased sensitivity of bone scintigraphy for the osteoblastic activity characteristic of prostate metastases [72, 79]. One advantage of PET is increased spatial resolution relative to bone scintigraphy. PET also has increased sensitivity relative to radiograph or CT, which do not permit reliable visualization of subtle marrow lesions, suggesting that PET might be an important tool in detecting metastases before morphologic changes are apparent by CT or CR [80]. Disadvantages of PET include relatively lower specificity, high cost, and lack of availability.

## *6.4 Skeletal Metastases of Unknown Origin*

In any particular patient, particularly an older patient, an aggressive lytic lesion of the skeleton is most likely to represent a metastatic lesion, given the relative rarity of primary bone malignancies. In patients with an unknown primary tumor, a protocol that includes screening with chest radiograph followed by CT of the torso (including chest, abdomen and pelvis) can identify 85 percent to 90 percent of primary tumors [81]. Employing mammography in the scenario in women with a tumor of unknown origin is controversial, particularly in the context of a normal

breast exam, since the yield of this additional test is uncertain. Importantly, biopsy of skeletal metastases often fails to identify the primary tumor, with undifferentiated or poorly differentiated carcinoma as the histologic diagnosis in up to 65 percent of cases [81].

### *6.5 Image-Guided Treatment of Painful Bone Metastases*

Treatment with external beam radiation is the current standard of care for patients with localized bone pain. Along with analgesics, chemotherapy, hormonal therapy and bisphosphonates, up to 70 percent of patients experience significant pain relief. Patients with spinal cord compression and a high life-expectancy may benefit from surgery, including debulking and vertebroplasty. However, the 30 percent of patients who are refractory to standard therapy provide a therapeutic challenge, and new image-guided treatment options, including radiofrequency ablation and cryoablation, show promise in helping this subgroup of patients (see below).

### *6.6 Summary of Bone Metastases*

Bone metastases are most commonly seen with cancers of the breast, prostate, lung, kidney, and thyroid gland, and characteristically present as multiple lesions in the axial skeleton of a patient over the age of 40. Imaging of bone metastases presents a diagnostic challenge due to their highly variable pathophysiology and radiologic appearance. Solitary lesions must be differentiated from primary bone tumors, while multiple lesions must be differentiated from multiple myeloma and lymphoma.

Treatment response can be very challenging to ascertain by all of the modalities due to the variable appearance of metastases and the variety of ways in which they respond. There are no current standardized criteria for following bone metastases, and these lesions are considered “non-target” lesions under the widely-used RECIST system.

## 7 Primary Bone Lymphoma

Primary bone lymphoma (PBL) is rare, accounting for only 5 percent of primary bone tumors (Figs. 15.12, 15.13). By definition these tumors are a diagnosis of exclusion and can only be considered when there is a focus of biopsy-proven lymphoma in a single bone, with no evidence of distal lymphatic or soft tissue involvement for six months. Regional lymph node involvement does not exclude a diagnosis of PBL. Non-Hodgkin’s Lymphomas represent the vast majority, usually

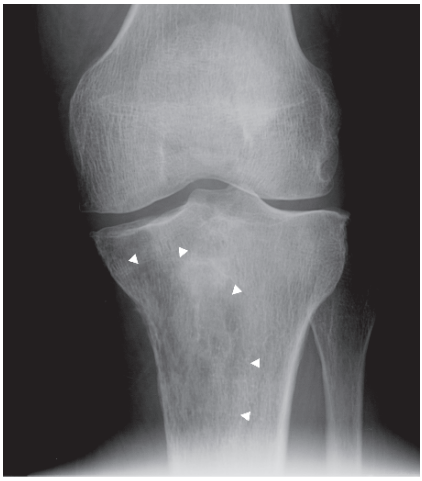

(a)

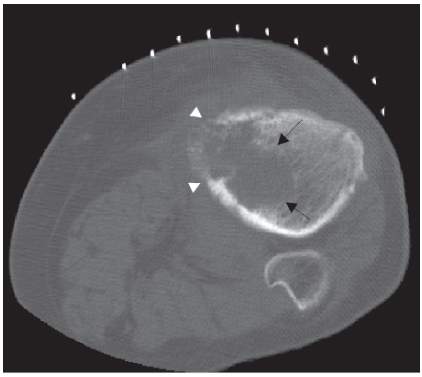

(b)

(c)

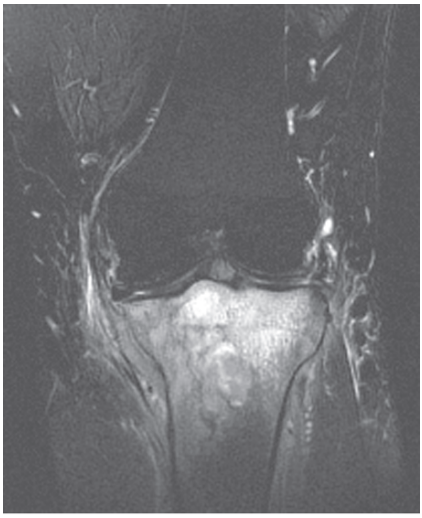

(d)

(e)

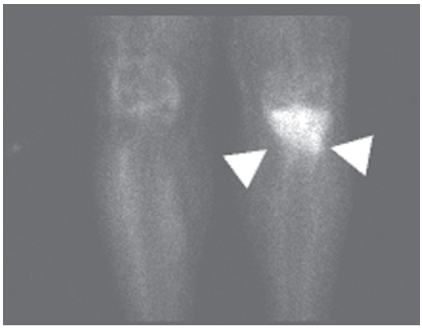

(f)

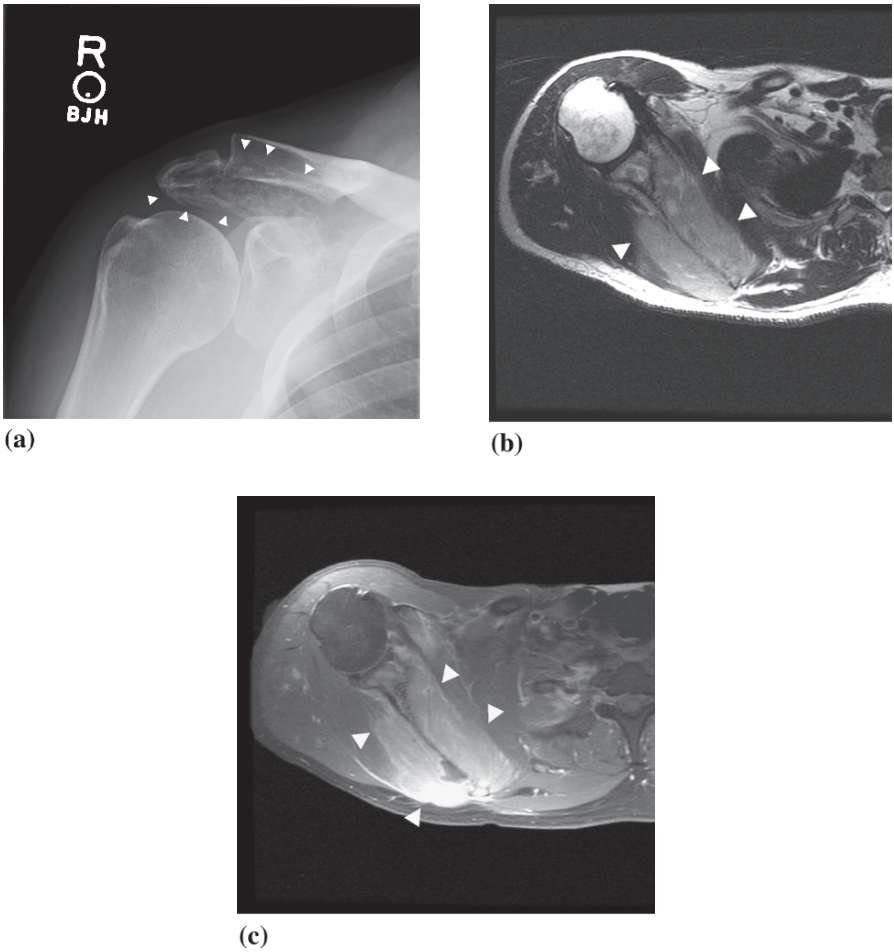


**Fig. 15.13** Lymphoma in a 36-year-old male. (**a**) Radiograph shows a permeative lesion involving the acromion and extending into the scapular body (arrowheads). (**b**) Axial T2 and (**c**) axial T1 post-gadolinium fat saturation MR images of the scapular body reveal a large soft tissue mass centered at the scapular body (arrowheads) that displaces the rotator cuff musculature

**Fig. 15.12** Primary lymphoma of bone in a 59-year-old female. (**a**) Frontal radiograph of the knee shows an ill-defined lytic lesion of the proximal tibia (arrowheads). (**b**) Axial CT scan performed at the time of percutaneous biopsy shows the lytic lesion with ill-defined margins (black arrows) and cortical destruction (white arrowheads). (**c**) Coronal proton density, (**d**) coronal STIR and (**e**) coronal post-gadolinium T1-weighted MR images of the proximal tibia show the lesion extending through the tibial cortex and to the articular surface of the proximal tibia. (**f**) Bone scintigraphy shows increased uptake in the proximal tibia, corresponding to the site of the lesion

of the large B-cell or mixed small and large B-cell lineage. Hodgkin's disease accounts for only 6 percent of cases [82]. There is a broad distribution of patients affected, ranging between 20 to 80 years old, with a peak prevalence in the sixth and seventh decades. Clinically, patients present with symptoms similar to many other primary bone tumors: either asymptomatically or with insidious bone pain or swelling. Rarely, systemic symptoms such as weight loss and fever can be present. Chemotherapy, with or without radiation, leads to a five-year survival of 83 percent to 90 percent. Younger patients with disease confined to a single location have a particularly excellent prognosis [83, 84]. Therefore, early radiographic detection and appropriate diagnosis is key. It is important to consider the possibility of lymphoma at the time of biopsy to ensure that appropriate cytologic analysis and immunophenotyping are performed during biopsy.

There is wide variability to the radiographic appearance of PBL, with certain features being more characteristic. A retrospective analysis from the AFIP of 237 pathologically proven cases of primary bone lymphoma revealed that 70 percent of lesions were lytic with 74 percent of these lesions showing a permeative or moth-eaten appearance; 71 percent of lesions occurred in the long bones; periosteal reaction was seen in 58 percent, commonly in a layered pattern; sequestra were found in 16 percent; and soft tissue masses were seen in 48 percent [82]. The metadiaphysis of the femur is, by far, the most common location for PBL, accounting for 25 percent of cases [83]. The metadiaphysis of the proximal tibia is also frequently involved. Cortical destruction, pathologic fractures, and large soft tissue masses indicate a more aggressive pattern and poorer prognosis [83]. Sclerosis can appear following therapy, leading to a mixed lytic and sclerotic appearance.

As primary lymphoma of the bone is a marrow-replacing process, findings can be subtle or even occult on radiography. If the patient has continued symptoms with a negative radiograph, a more sensitive study such as bone scintigraphy or MRI can be beneficial. On bone scintigraphy, primary bone lymphoma almost uniformly shows increased tracer uptake, reflecting increased osteoblastic activity. However, these findings are nonspecific and should be correlated with the radiographic findings.

MRI is the most sensitive modality for identifying and defining the extent of marrow involvement and soft tissue mass seen in PBL. Marrow replacement presents as low signal intensity on T1 with varied, though usually high, signal intensity on T2. Peritumoral edema also produces high T2 signal, while fibrosis within the lesion will decrease the T2 signal intensity. STIR images are particularly useful in showing the soft tissue mass. These lesions will also enhance following contrast administration [83].

The differential for PBL includes other permeative lesions such as osteosarcoma, metastatic disease, round cell tumors such as Ewing's Sarcoma and multiple myeloma, and secondary osseous lymphoma. Secondary osseous lymphoma can only be excluded after whole-body surveillance for distant lesions, either by PET or whole-body CT.

Finally, it is important to distinguish PBL from osteomyelitis. In the AFIP series, 16 percent of PBL cases had a sequestra, and 5 percent of cases had involve-

ment across the joint space to involve contiguous osseous structures, both of which are features that are more characteristic of infection [82]. Infection can be more definitively ruled out by a negative 99 mTc-WBC scintigraphy study. Clinical history is invaluable in narrowing the differential.

Chemotherapy is the mainstay of treatment, with or without adjuvant local radiation therapy, leading to survival rates of 83 percent to 90 percent. Follow-up after therapy is usually performed with MRI. Similar to other bone tumors, it is challenging to differentiate residual tumor from granulation tissue and necrosis. One series demonstrated a dramatic decrease in tumor volume in the first three months after initiation of therapy with 71 percent to 96 percent reduction by five months [84], with no change in signal characteristics of the lesion and no development of necrosis. Additionally, a pattern resembling bone infarct was observed following treatment, with a linear hypointense rim on T1 and adjacent high signal on T2-weighted images. Paralleling the tumor volume reduction, the soft tissue component almost universally disappeared by three to four months of therapy. The authors concluded that follow-up MRI should be performed at two to three months and six to 12 months after initiation of therapy [84].

Primary bone lymphoma is a rare entity, but should be considered for any adult with a solitary metadiaphyseal lesion in the distal femur, or proximal tibia that has a permeative lytic appearance with associated soft tissue mass and minimal cortical destruction. Work-up of these lesions include plain radiographs and MRI. Correct diagnosis is essential for early and appropriate treatment, which can lead to an excellent survival rate.

## 8 Ewing's Sarcoma

Ewing's sarcoma, a pediatric small round cell blue tumor, is the second most common primary bone malignancy in children and adolescents, after osteosarcoma. It is slightly more common in boys, with the second decade of life being the most common age of diagnosis. Whites are most commonly affected, while the tumor is rare in the African American population. Pain is the most common presenting symptom and is often attributed to bone growth or traumatic injury. Pain without trauma, continuing at night, and lasting over one month should prompt further work-up [85]. Tumor growth eventually leads to a palpable mass.

Most Ewing's sarcoma occur in bone, with the pelvic bones (26 percent), femur (20 percent), tibia/fibula (18 percent) and ribs (10 percent) most commonly involved. Unlike osteosarcoma, Ewing's sarcoma tends to originate in the diaphysis, rather then metaphysis. However, in clinical practice, localization in the metadiaphysis makes distinct classification difficult. Primary cranial, spinal (usually the sacrum or involving the posterior elements) and periosteal location without extension into the marrow is rare, but reported [86-88]. Primary metastasis to the lung, bone or bone marrow, or a combination of these sites is present in 25 percent of cases. Lymph node metastasis is rare [85].

The initial imaging modality for patients suspected of Ewing's is plain radiographs. Classically one will see an aggressive-appearing, permeative, diaphyseal lesion with a raised periosteum (Codman Triangle) or onion-skin periostitis, and calcifications within a surrounding soft tissue mass [85]. The differential of such a lesion in a child includes infection and eosinophilic granuloma, with a benign-appearing (thick, wavy) periosteal reaction suggesting eosinophilic granuloma (rare in Ewing's) and a bony sequestrum suggesting infection. A purely permeative lesion may not always be seen, as sclerotic reaction may also occur in response to the tumor, creating a more patchy lytic appearance.

Staging of Ewing's usually includes a chest CT, as lung or pleural involvement is the most frequent site of metastatic disease, bone marrow aspiration and a bone scan to detect occult skeletal lesions. Contrast-enhanced MRI may be used to assess bone marrow involvement or soft tissue extent, with non-contrast T1-weighted images shown to correlate best with tumor size on pathologic examination [89, 90]. MRI also appears to be the best modality to assess rare skip lesions in the bone, and may also be performed prior to biopsy to help guide biopsy [89]. It is suggested that MRI be performed prior to any procedure, as post-procedural changes can be confused with tumor involvement.

The use of FDG-PET is also becoming more frequent. PET and whole-body MRI have both been shown to detect more skeletal lesions than bone scan alone [90]. PET is slightly more sensitive than whole-body MRI in detecting skeletal lesions [90, 91]. The combination of whole-body MRI and bone scan may lead to results comparable with PET scanning alone, with less cost and fewer false positives [91]. Identifying distant lesions is important because they impact treatment protocols and are associated with poor prognosis (most notable for bone marrow metastasis) [85]. Confirmed local disease is amenable to surgery, while diffuse metastatic osseous disease will often alter the radiation therapy treatment plan.

Imaging is also playing a larger role in evaluating response to therapy. A small study indicated that FDG-PET correlates with histological response to neoadjuvant chemotherapy, and SUV values less then 2.5 in lesions after therapy have been shown to be predictive of progression-free survival, regardless of initial stage [92]. Timing of PET exam acquisition post-therapy has not been well-defined. Whether these results will alter management is also yet to be concluded, although early identification of non-responders may allow change in chemotherapy, and alteration of radiation therapy and surgical planning [90, 92]. MRI has also been evaluated to help monitor response to chemotherapy, especially after induction chemotherapy where post-therapy necrosis, currently determined following surgery, serves as a prognostic factor [93]. Work is currently being done to evaluate the efficacy of dynamic MRI, which utilizes the enhancement characteristics of tumors to help determine which tumors may respond to chemotherapy, and to correlate changes after chemotherapy with tumor necrosis [89, 93]. High-grade necrosis of tumor following induction therapy with wide, negative surgical margins have been shown to correlate with low local recurrence [93]. T2 signal variations in suspect lesions were initially thought to be correlated with good histologic response to therapy;

however, residual areas of viable Ewing's sarcoma have been found in areas with both low and high T2 signal [89].

Cure from Ewing's can only be achieved with chemotherapy and local control, with combination of multi-modality therapy resulting in cure rates of 50 percent or more in local disease. More widespread disease, often involving the bone or bone marrow, has a less than 20 percent chance of cure [85]. Other prognostic factors being evaluated include bone marrow micrometastasis and circulating tumor cells detected by reverse transcription PCR [89].

## 9 Image-Guided Procedures

### *9.1 Percutaneous Biopsy*

Percutaneous, image-guided biopsy of bone and soft tissue lesions is a widely used, minimally invasive, safe, and cost-effective approach to obtaining diagnostic tissue samples. The procedure can often be done with local anesthesia or moderate sedation, and has a low complication rate and rapid recovery time [94-96]. Most importantly, it can eliminate the need for open biopsy, which has been shown to have a 2 to 20 percent complication rate, allowing quicker treatment initiation [97, 98]. Complications can occur with percutaneous biopsy, and may be higher in nonspecialized oncology centers [94]. Conjoint planning and knowledge of compartmental anatomy cannot be over-emphasized, as adverse outcomes including unnecessary limb amputation have been documented following inappropriate percutaneous biopsy routes [97, 99-101]. Tumor cell seeding occurs rarely when compared to open biopsy, reinforcing the need to cooperatively plan the biopsy approach so there is no compromise of subsequent surgical procedure and needle track resection [94, 98, 102]. Indications include identification of primary or secondary tumors, metastasis or infection [94, 97]. There are few contraindications; important exceptions to this include the lack of an appropriate imaging approach ("target window"), overlying infection, and altered coagulation profile. Equally important is careful synthesis of available clinical and imaging information to avoid biopsy of classic benign ("do not touch") lesions [94].

Accuracy rates of both fine needle aspiration (FNA) and core biopsy in osteolytic, osteosclerotic and soft tissue lesions has been extensively reviewed, with accuracy/clinically useful rates using CT guidance of 66 percent to 97 percent, where accuracy of tissue sample was compared to that of final pathologic diagnosis or clinical follow-up, and "clinically useful" was defined as allowing initiation of correct treatment based on biopsy result [95, 103-105]. Diagnostic yield, providing a specimen that can be accurately interpreted by the examining pathologist, varies, but averages around 80 percent to 90 percent [96, 98]. Deep-seated or difficult to access lesions also appear amenable to CT-guided biopsy [96]. It is unclear if the site of the lesion affects accuracy [103, 106]. Immediate analysis of

FNA specimens by a cytopathology technologist allows immediate assessment of samples for tissue adequacy, thereby allowing increased diagnostic yield by prompting repeat sampling when necessary [97]. Some institutions have also demonstrated successful and accurate use of ultrasound in biopsy of select lesions. The key component in use of ultrasound in primary bone lesions is the corresponding presence of an extraosseous mass [107].

Completing both FNA and core biopsies helps to increase accuracy/clinically useful samples and reduces non-diagnostic samples. Limitations appear to exist most notably in a subset of patients with infectious etiology or tissue containing myxoid components [95, 103, 106]. It is not clear whether biopsy of bone lesions is more accurate than that of soft tissue lesions, with some recent reviews indicating better accuracy with bone lesions, and others displaying more accuracy with soft tissue lesions [95, 98, 103, 106]. Clinical suspicion still plays a large role in whether a patient is sent for an open biopsy; patients with accurate percutaneous biopsy results may still be sent for open biopsy because of a questionable diagnosis or low confidence in the needle biopsy result [95, 103, 108].

Examination of all imaging studies obtained in the patient is recommended, as MRI or ultrasound characteristics can help target areas that are most suspicious for malignancy and guide avoidance of necrotic or cystic areas that are likely to be low yield [100]. Decreased accuracy of needle biopsy, compared to open biopsy, is largely a result of the small sample size afforded by needle biopsy. This is of particular concern in heterogeneous lesions and well-differentiated lipomatous, chondroid, and cyst-like tumors that are difficult to distinguish from benign entities [94, 98]. In attempting to predict which lesions are best suited for a particular biopsy approach, some investigators have found that open biopsy is as unsuccessful in a similar group of tumors as needle biopsy, especially lesions that demonstrate prominent blood or fluid levels [97]. MRI-safe equipment and “interventional magnets” are not widespread, but where available may help increase diagnostic yield by allowing MRI- guided biopsy of suspicious regions [94, 107].

## *9.2 Image-Guided Therapy*

Percutaneous therapy is not limited to diagnosis, and treatment involving this approach has also increased. The target of percutaneous therapies is most commonly metastasis to bone, which has been shown to cause significant pain, decrease quality of life, lead to pathologic fractures, and induce depression and anxiety [109]. In the past, treatment for these lesions has been based on analgesics/opiates, local therapy (external beam radiation therapy or surgery), and systemic therapy (chemotherapy, hormonal, bisphosphonates) which usually proved effective [109]. However, 20 to 30 percent of patients treated with radiation do not experience pain relief. A recent multicenter trial revealed effectiveness in radiofrequency ablation in treatment of painful lytic or mixed lytic/blastic metastatic bone lesions from a multitude of cancers including renal, colorectal, lung, and thyroid carcinomas [109].

Radiofrequency ablation (RFA) involves transmitting a high-frequency alternating current through a needle to cause frictional heating and necrosis of tumor. Disadvantages of RFA include increased pain during and immediately following treatment and a period of weeks before substantial pain reduction is achieved [109, 110]. Cryoablation involves delivery of argon gas through an insulated probe, with rapid expansion of the gas resulting in cooling that reaches −100° C within a few seconds. Subsequent thawing is achieved by instilling helium gas, followied by another cycle of freezing. In a small single-center trial, Callstrom et al. showed results similar to RFA, with a significant reduction in pain levels in 14 patients [111]. Larger prospective multicenter trials need to be performed before either RFA or cryoablation become standard of care for therapeutically challenging patients. Percutaneous vertebroplasty is widely used and effective in treatment of painful pathologic vertebral body fractures [64].

With increased use and performance, it is expected that accuracy and yield of percutaneous-guided biopsy with fluoroscopy, CT, MRI or ultrasound will continue to improve. Development of external CT guidance localization devices may also make the procedure more accurate and easier to perform, while at the same time reducing procedural radiation doses [112].

## Key Points

- In summary, the available imaging modalities have benefits and limitations and therefore physicians must carefully select the correct test or set of tests to efficiently and accurately evaluate a patient that presents with a new skeletal lesion.
- Close interactions with the radiologist will ensure that patients are appropriately triaged.
- Given rapid changes in imaging technology and ongoing, active research in oncologic imaging, the future of skeletal tumor imaging promises many new innovations that will further expand the role of imaging in the diagnosis, staging, and treatment of patients in the future.

## References

1. Lodwick G S, Wilson A J, Farrell C, Virtama P, and Dittrich F. Determining growth rates of focal lesions of bone from radiographs. Radiology, *134:* 577-583, 1980.
2. Lodwick G S, Wilson A J, Farrell C, Virtama P, Smeltzer F M, and Dittrich F. Estimating rate of growth in bone lesions: observer performance and error. Radiology, *134:* 585-590, 1980.
3. Arndt C A and Crist W M. Common musculoskeletal tumors of childhood and adolescence. N Engl J Med, *341:* 342-352, 1999.
4. Murphey M D, Robbin M R, McRae G A, Flemming D J, Temple H T, and Kransdorf M J. The many faces of osteosarcoma. Radiographics, *17:* 1205-1231, 1997.
5. Miller S L and Hoffer F A. Malignant and benign bone tumors. Radiol Clin North Am, *39:* 673-699, 2001.

6. Sajadi K R, Heck R K, Neel M D, et al. The incidence and prognosis of osteosarcoma skip metastases. Clin Orthop Relat Res: 92-96, 2004.
7. Brenner W, Bohuslavizki K H, and Eary J F. PET imaging of osteosarcoma. J Nucl Med, *44:* 930-942, 2003.
8. Huvos A G, Rosen G, Bretsky S S, and Butler A. Telangiectatic osteogenic sarcoma: a clinicopathologic study of 124 patients. Cancer, *49:* 1679-1689, 1982.
9. Murphey M D, wan Jaovisidha S, Temple H T, Gannon F H, Jelinek J S, and Malawer M M. Telangiectatic osteosarcoma: radiologic-pathologic comparison. Radiology, *229:* 545-553, 2003.
10. Klein M J and Siegal G P. Osteosarcoma: anatomic and histologic variants. Am J Clin Pathol, *125:* 555-581, 2006.
11. Nakajima H, Sim F H, Bond J R, and Unni K K. Small cell osteosarcoma of bone. Review of 72 cases. Cancer, *79:* 2095-2106, 1997.
12. Jaffe H L. Intracortical osteogenic sarcoma. Bull Hosp Joint Dis, *21:* 189-197, 1960.
13. Smith J, Botet J F, and Yeh S D. Bone sarcomas in Paget disease: a study of 85 patients. Radiology, *152:* 583-590, 1984.
14. McCarville M B, Christie R, Daw N C, Spunt S L, and Kaste S C. PET/CT in the evaluation of childhood sarcomas. AJR Am J Roentgenol, *184:* 1293-1304, 2005.
15. Rodriguez-Galindo C, Shah N, McCarville M B, et al. Outcome after local recurrence of osteosarcoma: the St. Jude Children's Research Hospital experience (1970-2000). Cancer, *100:* 1928-1935, 2004.
16. Wittig J C, Bickels J, Priebat D, et al. Osteosarcoma: a multidisciplinary approach to diagnosis and treatment. Am Fam Physician, *65:* 1123-1132, 2002.
17. Imbriaco M, Yeh S D, Yeung H, et al. Thallium-201 scintigraphy for the evaluation of tumor response to preoperative chemotherapy in patients with osteosarcoma. Cancer, *80:* 1507-1512, 1997.
18. Menendez L R, Fideler B M, and Mirra J. Thallium-201 scanning for the evaluation of osteosarcoma and soft tissue sarcoma. A study of the evaluation and predictability of the histological response to chemotherapy. J Bone Joint Surg Am, *75:* 526-531, 1993.
19. Bredella M A, Caputo G R, and Steinbach L S. Value of FDG positron emission tomography in conjunction with MR imaging for evaluating therapy response in patients with musculoskeletal sarcomas. AJR Am J Roentgenol, *179:* 1145-1150, 2002.
20. Hawkins D S, Rajendran J G, Conrad E U, 3rd, Bruckner J D, and Eary J F. Evaluation of chemotherapy response in pediatric bone sarcomas by [F-18]-fluorodeoxy-D-glucose positron emission tomography. Cancer, *94:* 3277-3284, 2002.
21. Murphey M D, Walker E A, Wilson A J, Kransdorf M J, Temple H T, and Gannon F H. From the archives of the AFIP: imaging of primary chondrosarcoma: radiologic-pathologic correlation. Radiographics, *23:* 1245-1278, 2003.
22. Feldman F, Van Heertum R, Saxena C, and Parisien M. 18FDG-PET applications for cartilage neoplasms. Skeletal Radiol, *34:* 367-374, 2005.
23. Murphey M D, Flemming D J, Boyea S R, Bojescul J A, Sweet D E, and Temple H T. Enchondroma versus chondrosarcoma in the appendicular skeleton: differentiating features. Radiographics, *18:* 1213-1237; quiz 1244-1215, 1998.
24. Lee F Y, Yu J, Chang S S, Fawwaz R, and Parisien M V. Diagnostic value and limitations of fluorine-18 fluorodeoxyglucose positron emission tomography for cartilaginous tumors of bone. J Bone Joint Surg Am, *86-A:* 2677-2685, 2004.
25. Evans H L, Ayala A G, and Romsdahl M M. Prognostic factors in chondrosarcoma of bone: a clinicopathologic analysis with emphasis on histologic grading. Cancer, *40:* 818-831, 1977.
26. Arsos G, Venizelos I, Karatzas N, Koukoulidis A, and Karakatsanis C. Low-grade chondrosarcomas: a difficult target for radionuclide imaging. Case report and review of the literature. Eur J Radiol, *43:* 66-72, 2002.
27. Tallini G, Dorfman H, Brys P, et al. Correlation between clinicopathological features and karyotype in 100 cartilaginous and chordoid tumors. A report from the Chromosomes and Morphology (CHAMP) Collaborative Study Group. J Pathol, *196:* 194-203, 2002.

28. Janzen L, Logan P M, O'Connell J X, Connell D G, and Munk P L. Intramedullary chondroid tumors of bone: correlation of abnormal peritumoral marrow and soft tissue MRI signal with tumor type. Skeletal Radiol, *26:* 100-106, 1997.
29. Geirnaerdt M J, Bloem J L, Eulderink F, Hogendoorn P C, and Taminiau A H. Cartilaginous tumors: correlation of gadolinium-enhanced MR imaging and histopathologic findings. Radiology, *186:* 813-817, 1993.
30. Aoki J, Sone S, Fujioka F, et al. MRI of enchondroma and chondrosarcoma: rings and arcs of Gd-DTPA enhancement. J Comput Assist Tomogr, *15:* 1011-1016, 1991.
31. Geirnaerdt M J, Hogendoorn P C, Bloem J L, Taminiau A H, and van der Woude H J. Cartilaginous tumors: fast contrast-enhanced MR imaging. Radiology, *214:* 539-546, 2000.
32. Brenner W, Conrad E U, and Eary J F. FDG PET imaging for grading and prediction of outcome in chondrosarcoma patients. Eur J Nucl Med Mol Imaging, *31:* 189-195, 2004.
33. Collins M S, Koyama T, Swee R G, and Inwards C Y. Clear cell chondrosarcoma: radiographic, computed tomographic, and magnetic resonance findings in 34 patients with pathologic correlation. Skeletal Radiol, *32:* 687-694, 2003.
34. Kaim A H, Hugli R, Bonel H M, and Jundt G. Chondroblastoma and clear cell chondrosarcoma: radiological and MRI characteristics with histopathological correlation. Skeletal Radiol, *31:* 88-95, 2002.
35. Davila J A, Amrami K K, Sundaram M, Adkins M C, and Unni K K. Chondroblastoma of the hands and feet. Skeletal Radiol, *33:* 582-587, 2004.
36. Aoki J, Tanikawa H, Ishii K, et al. MRI findings indicative of hemosiderin in giant-cell tumor of bone: frequency, cause, and diagnostic significance. AJR Am J Roentgenol, *166:* 145-148, 1996.
37. Kumta S M, Griffith J F, Chow L T, and Leung P C. Primary juxtacortical chondrosarcoma dedifferentiating after 20 years. Skeletal Radiol, *27:* 569-573, 1998.
38. Schajowicz F. Juxtacortical chondrosarcoma. J Bone Joint Surg Br, *59-B:* 473-480, 1977.
39. Robinson P, White L M, Sundaram M, et al. Periosteal chondroid tumors: radiologic evaluation with pathologic correlation. AJR Am J Roentgenol, *177:* 1183-1188, 2001.
40. Seeger L L, Yao L, and Eckardt J J. Surface lesions of bone. Radiology, *206:* 17-33, 1998.
41. Antonescu C R, Argani P, Erlandson R A, Healey J H, Ladanyi M, and Huvos A G. Skeletal and extraskeletal myxoid chondrosarcoma: a comparative clinicopathologic, ultrastructural, and molecular study. Cancer, *83:* 1504-1521, 1998.
42. Amukotuwa S A, Choong P F, Smith P J, Powell G J, Thomas D, and Schlicht S M. Femoral mesenchymal chondrosarcoma with secondary aneurysmal bone cysts mimicking a small-cell osteosarcoma. Skeletal Radiol, *35:* 311-318, 2006.
43. Nussbeck W, Neureiter D, Soder S, Inwards C, and Aigner T. Mesenchymal chondrosarcoma: an immunohistochemical study of 10 cases examining prognostic significance of proliferative activity and cellular differentiation. Pathology, *36:* 230-233, 2004.
44. Chidambaram A and Sanville P. Mesenchymal chondrosarcoma of the maxilla. J Laryngol Otol, *114:* 536-539, 2000.
45. Nguyen B D, Daffner R H, Dash N, Rothfus W E, Nathan G, and Toca A R, Jr. Case report 790. Mesenchymal chondrosarcoma of the sacrum. Skeletal Radiol, *22:* 362-366, 1993.
46. Frassica F J, Unni K K, Beabout J W, and Sim F H. Dedifferentiated chondrosarcoma. A report of the clinicopathological features and treatment of seventy-eight cases. J Bone Joint Surg Am, *68:* 1197-1205, 1986.
47. Staals E L, Bacchini P, and Bertoni F. Dedifferentiated central chondrosarcoma. Cancer, *106:* 2682-2691, 2006.
48. Bruns J, Fiedler W, Werner M, and Delling G. Dedifferentiated chondrosarcoma–a fatal disease. J Cancer Res Clin Oncol, *131:* 333-339, 2005.
49. Littrell L A, Wenger D E, Wold L E, et al. Radiographic, CT, and MR imaging features of dedifferentiated chondrosarcomas: a retrospective review of 174 de novo cases. Radiographics, *24:* 1397-1409, 2004.
50. MacSweeney F, Darby A, and Saifuddin A. Dedifferentiated chondrosarcoma of the appendicular skeleton: MRI-pathological correlation. Skeletal Radiol, *32:* 671-678, 2003.

51. Okada K, Hasegawa T, Tateishi U, Endo M, and Itoi E. Dedifferentiated chondrosarcoma with telangiectatic osteosarcoma-like features. J Clin Pathol, *59:* 1200-1202, 2006.
52. Saifuddin A, Mann B S, Mahroof S, Pringle J A, Briggs T W, and Cannon S R. Dedifferentiated chondrosarcoma: use of MRI to guide needle biopsy. Clin Radiol, *59:* 268-272, 2004.
53. Mulligan M E. Imaging techniques used in the diagnosis, staging, and follow-up of patients with myeloma. Acta Radiol, *46:* 716-724, 2005.
54. Angtuaco E J, Fassas A B, Walker R, Sethi R, and Barlogie B. Multiple myeloma: clinical review and diagnostic imaging. Radiology, *231:* 11-23, 2004.
55. Durie B G, Kyle R A, Belch A, et al. Myeloma management guidelines: a consensus report from the Scientific Advisors of the International Myeloma Foundation. Hematol J, *4:* 379-398, 2003.
56. Vande Berg B C, Michaux L, Lecouvet F E, et al. Nonmyelomatous monoclonal gammopathy: correlation of bone marrow MR images with laboratory findings and spontaneous clinical outcome. Radiology, *202:* 247-251, 1997.
57. Baur A, Stabler A, Nagel D, et al. Magnetic resonance imaging as a supplement for the clinical staging system of Durie and Salmon? Cancer, *95:* 1334-1345, 2002.
58. Mulligan M E and Badros A Z. PET/CT and MR imaging in myeloma. Skeletal Radiol, *36:* 5-16, 2007.
59. Johnston C, Brennan S, Ford S, and Eustace S. Whole body MR imaging: applications in oncology. Eur J Surg Oncol, *32:* 239-246, 2006.
60. Lecouvet F E, Dechambre S, Malghem J, Ferrant A, Vande Berg B C, and Maldague B. Bone marrow transplantation in patients with multiple myeloma: prognostic significance of MR imaging. AJR Am J Roentgenol, *176:* 91-96, 2001.
61. Ghanem N, Lohrmann C, Engelhardt M, et al. Whole-body MRI in the detection of bone marrow infiltration in patients with plasma cell neoplasms in comparison to the radiological skeletal survey. Eur Radiol, *16:* 1005-1014, 2006.
62. Hartman R P, Sundaram M, Okuno S H, and Sim F H. Effect of granulocyte-stimulating factors on marrow of adult patients with musculoskeletal malignancies: incidence and MRI findings. AJR Am J Roentgenol, *183:* 645-653, 2004.
63. Lecouvet F E, Vande Berg B C, Michaux L, et al. Stage III multiple myeloma: clinical and prognostic value of spinal bone marrow MR imaging. Radiology, *209:* 653-660, 1998.
64. Layton K F, Thielen K R, Cloft H J, and Kallmes D F. Acute vertebral compression fractures in patients with multiple myeloma: evaluation of vertebral body edema patterns on MR imaging and the implications for vertebroplasty. AJNR Am J Neuroradiol, *27:* 1732-1734, 2006.
65. Erly W K, Oh E S, and Outwater E K. The utility of in-phase/opposed-phase imaging in differentiating malignancy from acute benign compression fractures of the spine. AJNR Am J Neuroradiol, *27:* 1183-1188, 2006.
66. Horger M, Claussen C D, Bross-Bach U, et al. Whole-body low-dose multidetector row-CT in the diagnosis of multiple myeloma: an alternative to conventional radiography. Eur J Radiol, *54:* 289-297, 2005.
67. Nandurkar D, Kalff V, Turlakow A, Spencer A, Bailey M J, and Kelly M J. Focal MIBI uptake is a better indicator of active myeloma than diffuse uptake. Eur J Haematol, *76:* 141-146, 2006.
68. Breyer R J, 3rd, Mulligan M E, Smith S E, Line B R, and Badros A Z. Comparison of imaging with FDG PET/CT with other imaging modalities in myeloma. Skeletal Radiol, *35:* 632-640, 2006.
69. Nanni C, Zamagni E, Farsad M, et al. Role of 18F-FDG PET/CT in the assessment of bone involvement in newly diagnosed multiple myeloma: preliminary results. Eur J Nucl Med Mol Imaging, *33:* 525-531, 2006.
70. Bredella M A, Steinbach L, Caputo G, Segall G, and Hawkins R. Value of FDG PET in the assessment of patients with multiple myeloma. AJR Am J Roentgenol, *184:* 1199-1204, 2005.
71. Moulopoulos L A, Gika D, Anagnostopoulos A, et al. Prognostic significance of magnetic resonance imaging of bone marrow in previously untreated patients with multiple myeloma. Ann Oncol, *16:* 1824-1828, 2005.

72. Ghanem N, Uhl M, Brink I, et al. Diagnostic value of MRI in comparison to scintigraphy, PET, MS-CT and PET/CT for the detection of metastases of bone. Eur J Radiol, *55:* 41-55, 2005.
73. Roodman G D. Mechanisms of bone metastasis. N Engl J Med, *350:* 1655-1664, 2004.
74. Hamaoka T, Madewell J E, Podoloff D A, Hortobagyi G N, and Ueno N T. Bone imaging in metastatic breast cancer. J Clin Oncol, *22:* 2942-2953, 2004.
75. Schweitzer M E, Levine C, Mitchell D G, Gannon F H, and Gomella L G. Bull's-eyes and halos: useful MRI discriminators of osseous metastases. Radiology, *188:* 249-252, 1993.
76. Spuentrup E, Buecker A, Adam G, van Vaals J J, and Guenther R W. Diffusion-weighted MR imaging for differentiation of benign fracture edema and tumor infiltration of the vertebral body. AJR Am J Roentgenol, *176:* 351-358, 2001.
77. Lauenstein T C, Goehde S C, Herborn C U, et al. Whole-body MR imaging: evaluation of patients for metastases. Radiology, *233:* 139-148, 2004.
78. Schmidt G P, Haug A R, Schoenberg S O, and Reiser M F. Whole-body MRI and PET-CT in the management of cancer patients. Eur Radiol, *16:* 1216-1225, 2006.
79. Fogelman I, Cook G, Israel O, and Van der Wall H. Positron emission tomography and bone metastases. Semin Nucl Med, *35:* 135-142, 2005.
80. Nakamoto Y, Cohade C, Tatsumi M, Hammoud D, and Wahl R L. CT appearance of bone metastases detected with FDG PET as part of the same PET/CT examination. Radiology, *237:* 627-634, 2005.
81. Rougraff B T, Kneisl J S, and Simon M A. Skeletal metastases of unknown origin. A prospective study of a diagnostic strategy. J Bone Joint Surg Am, *75:* 1276-1281, 1993.
82. Mulligan M E, McRae G A, and Murphey M D. Imaging features of primary lymphoma of bone. AJR Am J Roentgenol, *173:* 1691-1697, 1999.
83. Krishnan A, Shirkhoda A, Tehranzadeh J, Armin A R, Irwin R, and Les K. Primary bone lymphoma: radiographic-MR imaging correlation. Radiographics, *23:* 1371-1383; discussion 1384-1377, 2003.
84. Mengiardi B, Honegger H, Hodler J, Exner U G, Csherhati M D, and Bruhlmann W. Primary lymphoma of bone: MRI and CT characteristics during and after successful treatment. AJR Am J Roentgenol, *184:* 185-192, 2005.
85. Bernstein M, Kovar H, Paulussen M, et al. Ewing's sarcoma family of tumors: current management. Oncologist, *11:* 503-519, 2006.
86. Hatori M, Okada K, Nishida J, and Kokubun S. Periosteal Ewing's sarcoma: radiological imaging and histological features. Arch Orthop Trauma Surg, *121:* 594-597, 2001.
87. Ilaslan H, Sundaram M, Unni K K, and Dekutoski M B. Primary Ewing's sarcoma of the vertebral column. Skeletal Radiol, *33:* 506-513, 2004.
88. Li W Y, Brock P, and Saunders D E. Imaging characteristics of primary cranial Ewing sarcoma. Pediatr Radiol, *35:* 612-618, 2005.
89. Brisse H, Ollivier L, Edeline V, et al. Imaging of malignant tumours of the long bones in children: monitoring response to neoadjuvant chemotherapy and preoperative assessment. Pediatr Radiol, *34:* 595-605, 2004.
90. Furth C, Amthauer H, Denecke T, Ruf J, Henze G, and Gutberlet M. Impact of whole-body MRI and FDG-PET on staging and assessment of therapy response in a patient with Ewing sarcoma. Pediatr Blood Cancer, *47:* 607-611, 2006.
91. Daldrup-Link H E, Franzius C, Link T M, et al. Whole-body MR imaging for detection of bone metastases in children and young adults: comparison with skeletal scintigraphy and FDG PET. AJR Am J Roentgenol, *177:* 229-236, 2001.
92. Hawkins D S, Schuetze S M, Butrynski J E, et al. [18F]Fluorodeoxyglucose positron emission tomography predicts outcome for Ewing sarcoma family of tumors. J Clin Oncol, *23:* 8828-8834, 2005.
93. Dyke J P, Panicek D M, Healey J H, et al. Osteogenic and Ewing sarcomas: estimation of necrotic fraction during induction chemotherapy with dynamic contrast-enhanced MR imaging. Radiology, *228:* 271-278, 2003.
94. Choi J J, Davis K W, and Blankenbaker D G. Percutaneous musculoskeletal biopsy. Semin Roentgenol, *39:* 114-128, 2004.

95. Ogilvie C M, Torbert J T, Finstein J L, Fox E J, and Lackman R D. Clinical utility of percutaneous biopsies of musculoskeletal tumors. Clin Orthop Relat Res, *450:* 95-100, 2006.
96. Puri A, Shingade V U, Agarwal M G, et al. CT-guided percutaneous core needle biopsy in deep seated musculoskeletal lesions: a prospective study of 128 cases. Skeletal Radiol, *35:* 138-143, 2006.
97. Jelinek J S, Murphey M D, Welker J A, et al. Diagnosis of primary bone tumors with image-guided percutaneous biopsy: experience with 110 tumors. Radiology, *223:* 731-737, 2002.
98. Mitsuyoshi G, Naito N, Kawai A, et al. Accurate diagnosis of musculoskeletal lesions by core needle biopsy. J Surg Oncol, *94:* 21-27, 2006.
99. Anderson M W, Temple H T, Dussault R G, and Kaplan P A. Compartmental anatomy: relevance to staging and biopsy of musculoskeletal tumors. AJR Am J Roentgenol, *173:* 1663-1671, 1999.
100. Liu P T, Valadez S D, Chivers F S, Roberts C C, and Beauchamp C P. Anatomically based guidelines for core needle biopsy of bone tumors: implications for limb-sparing surgery. Radiographics, *27:* 189-205; discussion 206, 2007.
101. Mankin H J, Mankin C J, and Simon M A. The hazards of the biopsy, revisited. Members of the Musculoskeletal Tumor Society. J Bone Joint Surg Am, *78:* 656-663, 1996.
102. Davies N M, Livesley P J, and Cannon S R. Recurrence of an osteosarcoma in a needle biopsy track. J Bone Joint Surg Br, *75:* 977-978, 1993.
103. Hau A, Kim I, Kattapuram S, et al. Accuracy of CT-guided biopsies in 359 patients with musculoskeletal lesions. Skeletal Radiol, *31:* 349-353, 2002.
104. Leffler S G and Chew F S. CT-guided percutaneous biopsy of sclerotic bone lesions: diagnostic yield and accuracy. AJR Am J Roentgenol, *172:* 1389-1392, 1999.
105. Stoker D J, Cobb J P, and Pringle J A. Needle biopsy of musculoskeletal lesions. A review of 208 procedures. J Bone Joint Surg Br, *73:* 498-500, 1991.
106. Tsukushi S, Katagiri H, Nakashima H, Shido Y, and Arai E. Application and utility of computed tomography-guided needle biopsy with musculoskeletal lesions. J Orthop Sci, *9:* 122-125, 2004.
107. Saifuddin A, Mitchell R, Burnett S J, Sandison A, and Pringle J A. Ultrasound-guided needle biopsy of primary bone tumours. J Bone Joint Surg Br, *82:* 50-54, 2000.
108. Yao L, Nelson S D, Seeger L L, Eckardt J J, and Eilber F R. Primary musculoskeletal neoplasms: effectiveness of core-needle biopsy. Radiology, *212:* 682-686, 1999.
109. Goetz M P, Callstrom M R, Charboneau J W, et al. Percutaneous image-guided radiofrequency ablation of painful metastases involving bone: a multicenter study. J Clin Oncol, *22:* 300-306, 2004.
110. Callstrom M R, Charboneau J W, Goetz M P, et al. Painful metastases involving bone: feasibility of percutaneous CT- and US-guided radio-frequency ablation. Radiology, *224:* 87-97, 2002.
111. Callstrom M R, Atwell T D, Charboneau J W, et al. Painful metastases involving bone: percutaneous image-guided cryoablation–prospective trial interim analysis. Radiology, *241:* 572-580, 2006.
112. Roberts C C, Morrison W B, Deely D M, Zoga A C, Koulouris G, and Winalski C S. Use of a novel percutaneous biopsy localization device: initial musculoskeletal experience. Skeletal Radiol, *36:* 53-57, 2007.